(2)

**Naval Research Laboratory**

Washington, DC 20375-5000

NRL Memorandum Report 6294



# Electron Collision Shift of the Lyman-Alpha Line In H and $He^+$

M. BLAHA

*Laboratory for Plasma Research*
*University of Maryland*
*College Park, MD 20742*

J. DAVIS

*Plasma Radiation Branch*
*Plasma Physics Division*

September 9, 1988

SECURITY CLASSIFICATION OF THIS PAGE

AD-A200 296

# REPORT DOCUMENTATION PAGE

Form Approved
OMB No. 0704-0188

| | |
|---|---|
| 1a. REPORT SECURITY CLASSIFICATION<br>UNCLASSIFIED | 1b. RESTRICTIVE MARKINGS |
| 2a. SECURITY CLASSIFICATION AUTHORITY | 3. DISTRIBUTION/AVAILABILITY OF REPORT<br>Approved for public release; distribution unlimited. |
| 2b. DECLASSIFICATION/DOWNGRADING SCHEDULE | |
| 4. PERFORMING ORGANIZATION REPORT NUMBER(S)<br>NRL Memorandum Report 6294 | 5. MONITORING ORGANIZATION REPORT NUMBER(S) |
| 6a. NAME OF PERFORMING ORGANIZATION<br>Naval Research Laboratory | 6b. OFFICE SYMBOL (If applicable)<br>Code 4720 |
| 6c. ADDRESS (City, State, and ZIP Code)<br>Washington, DC 20375-5000 | 7a. NAME OF MONITORING ORGANIZATION |
| 7b. ADDRESS (City, State, and ZIP Code) | |
| 8a. NAME OF FUNDING/SPONSORING ORGANIZATION<br>Office of Naval Research | 8b. OFFICE SYMBOL (If applicable) |
| 8c. ADDRESS (City, State, and ZIP Code)<br>Arlington, VA 22217 | 9. PROCUREMENT INSTRUMENT IDENTIFICATION NUMBER |
| | 10. SOURCE OF FUNDING NUMBERS<br>PROGRAM ELEMENT NO: 61153N; PROJECT NO:; TASK NO: RR011-09-41; WORK UNIT ACCESSION NO: DN080-035 |

11. TITLE (Include Security Classification)
Electron Collision Shift of the Lyman-Alpha Line in H and $He^+$

12. PERSONAL AUTHOR(S)
Blaha, M. and Davis, J.

| 13a. TYPE OF REPORT | 13b. TIME COVERED | 14. DATE OF REPORT (Year Month Day) | 15. PAGE COUNT |
|---|---|---|---|
| Interim | FROM _____ TO _____ | 1988 September 9 | 55 |

16. SUPPLEMENTARY NOTATION
This work was supported by the Office of Naval Research

| 17. COSATI CODES | | |
|---|---|---|
| FIELD | GROUP | SUB GROUP |
| | | |
| | | |

18. SUBJECT TERMS (Continue on reverse if necessary and identify by block number)

19. ABSTRACT (Continue on reverse if necessary and identify by block number)

The sensitivity of spectral line shift is investigated in the impact approximation for a variety of assumptions using the distorted-wave with exchange approach. The formalism is applied to the Lyman-alpha line of hydrogen and ionized helium to determine the influence of various assumptions on the line shift as well as identifying the differences between a neutral and ionized radiator. The results are compared and contrasted with a number of other calculations and experimental measurements. (AU)

| 20. DISTRIBUTION/AVAILABILITY OF ABSTRACT | 21. ABSTRACT SECURITY CLASSIFICATION |
|---|---|
| [X] UNCLASSIFIED/UNLIMITED [ ] SAME AS RPT [ ] DTIC USERS | UNCLASSIFIED |
| 22a. NAME OF RESPONSIBLE INDIVIDUAL<br>Dr. Jack Davis | 22b. TELEPHONE (Include Area Code)<br>(202) 767-3278 |
| | 22c. OFFICE SYMBOL<br>Code 4720 |

DD Form 1473, JUN 86 Previous editions are obsolete SECURITY CLASSIFICATION OF THIS PAGE

S/N 0102-LF-014-6603

## CONTENTS

# ELECTRON COLLISION SHIFT OF THE LYMAN-ALPHA LINE IN H AND $HE^+$

## I. Introduction

The interaction of plasma microfields with radiating atoms and ions causes a line broadening that governs both the the half-width and shift of the spectral line, i.e., the intensity distribution in frequency is altered to reflect the presence of the plasma. The line shifts are of particular interest both for their intrinsic value in terms of providing insight into the fundamental nature of the underlying physical processes affecting the emission of radiation as well as its diagnostic value in the study of high density plasmas. In addition, exact wavelengths of spectral lines of highly charged ions are required in the determination of line opacities and level positions for x-ray laser transitions.

Since the first investigation by Berg, et al.[1] on the effects of plasma interactions on the frequency shift of spectral lines it still remains an interesting and challenging problem. This is due primarily to its N-body nature for which only approximate solutions can be found. However, in low density plasmas the mutual interactions of perturbing particles may be neglected converting an intractable problem into a manageable one, making it possible to evaluate line profiles in the impact approximation via the Baranger formalism.[2] This theory is based on the knowledge of the scattering matrix for collisions of electrons and the radiator in the upper as well as in the lower state of the line. In the application of Baranger's theory, the initial perturber-radiator correlations are generally neglected, and the theory leads to negative (i.e. red) frequency shifts of Lyman-alpha lines of hydrogen-like ions[3,4], contrary to experimental results[5-8] which yield blue shifts. It has been suggested[9] that another effect which is associated with initial perturber-radiator correlations, namely plasma polarization, may cause blue shifts of hydrogen-like lines. Plasma polarization effects on $He^+$ lines have been calculated by several authors[5-8,10] with the assumption of charge neutrality outside the orbit of the bound electron with the result of blue line-shifts. However, a procedure similar to the quantum-mechanical approach of Volonte'[10], but with inclusion of electric charges in the outer region, leads again to red shifts of Lyman lines.[11]

In the present investigation, we concentrate our efforts on a few special problems in the theory of the line-shift, mainly the sensitivity of calculated shifts to various effects taken into account in the evaluation of

Manuscript approved July 12, 1988.

scattering matrices. For this reason we have chosen the Lyman-alpha lines of hydrogen and of ionized helium as two typical examples where the effects can be demonstrated and differences between a neutral and an ionized emitter may be seen. Our approach is fully quantum-mechanical, and the scattering matrices are obtained in a distorted-wave approximation with exchange. This approximation, although rather simple, is convenient for our purposes because it is very well suited for the calculation of various effects - addition or deletion of different terms in the scattering matrix can be performed easily. We calculated only the electron collision contributions to the shift. Effects of plasma ions will be neglected. Our basic assumption is that perturber-perturber interactions are weak and can be ignored, and therefore the applicability of the results is limited to low-density plasmas, where the Debye shielding length is much larger than the dimensions of the radiator, i.e. for $N_e < 10^{18}$ cm$^{-3}$. However, the effect of shielding has to be taken into account even at the low density limit for perturbing collisions involving the $\Delta n=0$ transitions and it will be separately discussed in par. II.4.

The quantum-mechanical results are then compared to line-shifts derived from considerations based on the electrostatic interaction of the bound electron with the plasma. It will be shown that at the limit of weak interaction, both results are identical, but that neither in hydrogen nor in $He^+$ has this limit been reached.

## II. Calculation of the Lyman-alpha line shift using the scattering matrix formalism.

The shift of the Lyman-alpha line of hydrogen and ionized helium produced by electron collisions will be calculated with the assumption that the impact approximation is valid, which means that results will be applicable to low-density plasmas only. We will also assume that: 1) the perturber-perturber interactions are small and can be neglected, 2) the wave functions of the bound electron are not changed by plasma interactions, and 3) we will ignore the effect of positive ions. No uniform positive background will be included in the calculations, and the fine structure splitting of atomic levels will be neglected. All calculated shifts will be normalized to the electron density $N_e=1$ cm$^{-3}$. Unless indicated otherwise, all quantities throughout the paper will be given in atomic units ($e=h/2\pi=m=1$).

Within the validity of the impact approximation, the electron collision profile of a spectral line is determined by electron scattering on the upper and the lower level of the line. Let us denote by $\bar{\ell}$ and $\ell$ the orbital quantum number of the bound and the colliding electron, respectively, and by a subscript p or s all quantities associated with the scattering on the upper or lower level. The scattering on the upper level $n_p\bar{\ell}_p$ is characterized by elements of the scattering matrix $S(\alpha_p, \alpha_p')$, where the scattering channels $\alpha_p$, $\alpha_p'$ are defined by

$$\alpha_p \equiv n_p\bar{\ell}_p k_p \ell_p L_p S_p ,$$

$$\alpha_p' \equiv n_p'\bar{\ell}_p' k_p' \ell_p' L_p S_p .$$

$k_p$ ($k_p'$) = momentum of the colliding electron before (after) the collision, $L_p S_p$ = total orbital and spin angular momentum. Similarly, for the scattering on the lower level $n_s\bar{\ell}_s$ we have

$$\alpha_s = n_s\bar{\ell}_s k_s \ell_s L_s S_s ,$$

$$\alpha_s' = n_s'\bar{\ell}_s' k_s' \ell_s' L_s S_s .$$

For the Lyman-alpha line,

$$n_p\bar{\ell}_p \equiv 2p,\ L_p = \ell_p,\ \ell_p \pm 1,\ S_p = 0,\ 1,$$

$$n_s\bar{\ell}_s \equiv 1s,\ L_s = \ell_s,\ S_s = 0,\ 1.$$

According to Baranger[2], the angular frequency shift $\Delta\omega$ of the radiative transition $n_p p \rightarrow n_s s$ is proportional to the electron density $N_e$ and it can be expressed in terms of diagonal elements of the scattering matrix $S(\alpha_p, \alpha_p)$ and $S(\alpha_s, \alpha_s)$ by

$$\Delta\omega = \frac{1}{12}\ \pi N_e \int k^{-1} f(k) \sum_{\ell, L_p, S^T} (2L_p + 1)$$

$$x(2S^T + 1)\ \mathrm{Im}\left[1 - S\left(\alpha_p, \alpha_p\right) S^*\left(\alpha_s, \alpha_s\right)\right] dk \qquad (1)$$

with $k=k_p=k_s$, $S^T=S_p=S_s$, $\ell=\ell_p=\ell_s$ . $f(k)$ is the momentum distribution function of plasma electrons which is represented by a Maxwellian distribution in the present calculation.

For each value of $\ell$ and $S^T$ (and consequently for each matrix element $S(\alpha_s, \alpha_s)$), the sum over $L_p$ has three terms with different elements $S(\alpha_p, \alpha_p)$. A schematic example of diagonal matrix elements $S(\alpha_p, \alpha_p)$ for total angular momenta $L_p=1,2,3$ and one particular value of $S^T$ is shown on Fig. 1. Elements with $\ell=2$, corresponding to different terms in the sum over $L_p$, are indicated by X.

It is convenient to rewrite (1) in terms of transmission matrices $\underset{\sim}{T}$. From the relation $\underset{\sim}{T} = 1 - \underset{\sim}{S}$ it follows

$$1 - S(\alpha_p, \alpha_p)S^*(\alpha_s, \alpha_s) = T(\alpha_p, \alpha_p) + T^*(\alpha_s, \alpha_s) - T(\alpha_p, \alpha_p)T^*(\alpha_s, \alpha_s) \qquad (2)$$

and the total line-shift is thus decomposed into two parts: contributions from direct terms $T(\alpha_p, \alpha_p) + T^*(\alpha_s, \alpha_s)$ and from the interference term $- T(\alpha_p, \alpha_p)\ T^*(\alpha_s, \alpha_s)$.

II.1 Evaluation of the $\underset{\sim}{T}$ matrix for ionized helium and hydrogen.

In the evaluation of diagonal elements of the transmission matrix $\underset{\sim}{T}$ it is generally necessary to take into account coupling of several scattering channels. However, in the case of the Lyman-alpha line, the energy difference between the n=1 and n=2 levels in hydrogen and $He^+$ is much larger than the average kinetic energy of plasma electrons at the temperatures considered in our calculation, so that only a very small fraction of electrons scattered from the 1s level are affected by coupling to other channels. Therefore, we simplify our procedure by omitting all other levels in the evaluation of the matrix elements $T(\alpha_s, \alpha_s)$. On the other hand, we

have included levels 1s, 2s, 2p, 3s, 3p, 3d in the $\underset{\sim}{T}$ matrix for the evaluation of $T(\alpha_p, \alpha_p)$, but we have ignored all elements which do not involve the 2p level and consequently have only a small indirect effect on $T(\alpha_p, \alpha_p)$. The structure of a $\underset{\sim}{T}$ matrix used for the evaluation of diagonal elements corresponding to one particular value of $L_p$ and $S^T$ is shown on Fig. 2. Matrix elements taken into account in our calculation are marked by X.

All matrix elements $S(\alpha, \alpha')$ have been calculated in the distorted wave approximation with exchange (DWX). In the following we give a brief outline of the procedure.

First, we calculate the $\underset{\sim}{\rho}$ matrix[12] with elements defined by

$$\rho(\alpha,\alpha') = -2\Big[\Big(1-\delta_{\alpha\alpha'}\Big)\, f_o\Big(\bar{\ell}\ \ell\ \bar{\ell}'\ \ell'\ L^T\Big)\, R_o^d\Big(\bar{\ell}\ \ell\ \bar{\ell}'\ \ell'\Big)$$

$$+ \sum_{\lambda=1}^{\infty} f_\lambda\Big(\bar{\ell}\ \ell\ \bar{\ell}'\ \ell'\ L^T\Big)\, R_\lambda^d\Big(\bar{\ell}\ \ell\ \bar{\ell}'\ \ell'\Big)$$

$$+ (-1)^{S^T} \sum_{\lambda=0}^{\infty} g_\lambda\Big(\bar{\ell}\ \ell\ \bar{\ell}'\ \ell'\ L^T\Big)\ R_\lambda^e\Big(\bar{\ell}\ \ell\ \bar{\ell}'\ \ell'\Big)\Big] \quad . \tag{3}$$

$\bar{\ell}$ and $\bar{\ell}'$ are the orbital angular momenta of the bound electron before and after the collision, $\ell$ and $\ell'$ correspond to the colliding electron, $L^T$ and $S^T$ are the total orbital and spin angular momenta of the system with $L^T = L_p$ or $L_s$, $f_\lambda(\bar{\ell}\ \ell\ \bar{\ell}'\ \ell'\ L^T)$ and $g_\lambda(\bar{\ell}\ \ell\ \bar{\ell}'\ \ell'\ L^T)$ are coefficients given by Percival and Seaton.[13]

The direct and the exchange radial integrals $R_\lambda^d$ and $R_\lambda^e$ are defined by

$$R_\lambda^d = \int P\Big(n\bar{\ell};\ r_1\Big)\, F_{k\ell}\Big(r_2\Big)\ \frac{r_<^\lambda}{r_>^{\lambda+1}}\ \Big(P\ n'\bar{\ell}';r_1\Big)\, F_{k'\ell'}\Big(r_2\Big)\, dr_1 dr_2, \tag{4}$$

$$R_\lambda^e = \int P\Big(n\bar{\ell};\ r_1\Big)\, F_{k\ell}\Big(r_2\Big)\ \frac{r_<^\lambda}{r_>^{\lambda+1}}\ \Big(P\ n'\bar{\ell}';\ r_2\Big)\, F_{k'\ell'}\ \Big(r_1\Big)\, dr_1\, dr_2 \quad . \tag{5}$$

$r_<$ is the lesser and $r_>$ the greater of $r_1$ and $r_2$, $P(n\bar{\ell}; r)$ and $P(n'\bar{\ell}'; r)$ are the radial wave functions of the bound electron before and after the collision normalized to unity, and $F_{k\ell}$ is the radial function of the colliding electron before the collision satisfying the equation

$$\left[\frac{d^2}{dr^2} - \frac{\ell(\ell+1)}{r^2} + \frac{2(Z+1)}{r} - 2V\left(n\bar{\ell}; r\right) + k^2\right] F_{k\ell}(r)$$

$$= C\, P\left(n\bar{\ell}; r\right) + C'\, P\left(n'\bar{\ell}'; r\right), \tag{6}$$

$$V(n\bar{\ell}; r) = \int \frac{1}{r_>} P^2\left(n\bar{\ell}; r_1\right) dr_1 \ , \quad r_> \text{ being the greater of } r \text{ and } r_1. \tag{7}$$

$V(n\bar{\ell}; r)$ represents the monopole part of the electrostatic interaction energy of the bound and the free electron. Z is the asymptotic charge for the colliding electron and Lagrange multipliers C, C' are non-zero only if $\ell=\bar{\ell}$ or $\ell=\bar{\ell}'$, respectively. They are determined so that the functions $P(n\ell; r)$ and $P(n'\bar{\ell}'; r)$ are orthogonal to $F_{k\ell}(r)$, i.e.

$$\int P\left(n\bar{\ell}; r\right) F_{k\ell}\left(r\right) dr = \int P\left(n'\bar{\ell}'; r\right) F_{k\ell}\left(r\right) dr = 0 \ . \tag{8}$$

The asymptotic form of $F_{k\ell}$ is

$$F_{k\ell}\left(r\right) \sim k^{-1/2} \sin\left[kr - \frac{1}{2}\ell\pi + \frac{Z}{k}\ell n\left(2kr\right) + \arg\Gamma\left(\ell + 1 - \frac{iZ}{k}\right) + \tau_\alpha\right] . \tag{9}$$

The phase shift $\tau_\alpha$ depends on k, $\ell$, and on the level $n\bar{\ell}$, but it is independent of $L^T$, $S^T$.

Radial functions $F_{k'\ell'}$ of the scattered electron are calculated in a similar way.

From $\underset{\sim}{\rho}$ we obtain the matrix $\underset{\sim}{S}'$ using

$$\underset{\sim}{S}' = (1 + i\underset{\sim}{\rho})\ (1 - i\underset{\sim}{\rho})^{-1} \ . \qquad (10)$$

The $\underset{\sim}{S}'$ matrix and the scattering matrix $\underset{\sim}{S}$ are related by

$$\underset{\sim}{S} = e^{i\tau}\ \underset{\sim}{S}'\ e^{i\tau} \ , \qquad (11)$$

$e^{i\tau}$ being diagonal matrices with elements $e^{i\tau_\alpha}$ . The diagonal elements of the transmission matrix are then given by

$$T(\alpha, \alpha) = 1 - S'(\alpha, \alpha)\ e^{2i\tau_\alpha} \ . \qquad (12)$$

In the present version of the distorted-wave approximation, the channels included in the $\underset{\sim}{\rho}$ matrix are uncoupled. However, transformation (10) introduces a certain amount of coupling into the scattering matrix $\underset{\sim}{S}$, and consequently the line-shift calculated from eq. (1) depends on the number of levels included in the $\underset{\sim}{\rho}$ and $\underset{\sim}{S}$ matrices.

In the summation over $\ell$ in eq. (1), we have included values up to $\ell$=13. Sufficient convergence was achieved for the case of $He^+$, for hydrogen we have extrapolated partial contributions to the shift assuming their proportionality to $\ell^{-q}$ and determined q from values for $\ell$=12 and 13. The extrapolated contributions were always less than 5% of the total shift.

Values of $T(\alpha_p, \alpha_p)$ and $T(\alpha_s, \alpha_s)$ have been obtained for 10 different energies $^1/_2\ k^2$ of the colliding electron. The energy mesh was determined so that it would give the best possible accuracy of the integral over the velocity distribution, and at the same time it would take into account the discontinuity of $T(\alpha_p, \alpha_p)$ at the excitation threshold of the n=3 levels. No resonance effects below the n=3 threshold were taken into account in our procedure.

The shifts for the Lyman-alpha line have been calculated for electron temperatures corresponding to 2.0, 2.5, 3.0 and 4.0 eV for $He^+$, and to 0.5, 1.0, 1.5 and 2.0 eV for hydrogen.

If the diagonal matrix elements of $\underset{\sim}{S}$ are much larger than the off-diagonal elements, the scattering may be approximately treated as a one-channel problem. In this case

$$S(\alpha, \alpha) = e^{2i\eta_\alpha} \tag{13}$$

and the phase shift $\eta_\alpha$ in our approximation is given by

$$\eta_\alpha = \tau_\alpha + 1/2 \arctan[2\rho(\alpha, \alpha)/\{1 - \rho^2(\alpha, \alpha)\}] \tag{14}$$

according to (10) and (11). Equation (13) indicates the importance of phase shifts $\eta_\alpha$ for the calculation of frequency shifts $\Delta\omega$.

The accuracy of phase shifts $\eta_\alpha$ obtained from (14) may be illustrated by a comparison with values calculated by Oza[14] using a pseudo-state close-coupling method for scattering on the 1s state of the $He^+$ which is shown in Figs. 3-5. Oza's method is substantially more accurate than our simple DWX approximation, but the differences of the two results represent not only the differences of the two methods, but also the fact that his phase shifts are affected by coupling to other channels so that (13) is generally not valid. This explains why the smallest relative differences occur for $\ell$=0 (S-wave) with the largest phase shift. Apparently, the major contribution to the phase shift comes from pure elastic scattering, therefore (13) is approximately satisfied even for Oza's values of the shift, and the discrepancy may be caused just by the difference of methods. As the elastic scattering decreases with increasing $\ell$, coupling to other channels becomes more important and the comparison of the two quantities eventually becomes meaningless.

## II.2 Results.

One of the goals of this investigation was to establish the importance of different contributions to the total line-shift. Therefore we have performed a series of calculations in which certain terms were omitted in the expression for $\Delta\omega$. A list of all calculations is shown on Table 1, and results of the distorted-

wave approximation are presented on Figs. 6 and 7 for $He^+$ and on Figs. 10-12 for hydrogen. In both cases we have found red line shifts.

Curve A on Figs. 6-13 represents the most complete DWX calculation with all levels 1s-3d included in the $\underset{\sim}{S}$ matrix as described in par. II.1.

For $He^+$ (Fig. 6), the omission of levels 3s, 3p, 3d leads to curve D, which indicates that the higher levels have only a very small effect on the frequency shift of Lyman-alpha line. If only 1s and 2p levels are included, the results is given by B, and if, in addition, all exchange terms are omitted and only elastic terms retained, the shift is represented by C. A glance at Fig. 6 and comparison of A and C shows that the pure elastic scattering is by far the most important contribution to the frequency shift. In this particular case $\Delta\omega$ depends only on phase shifts $\tau_\alpha$, because $\underset{\sim}{\rho} = 0$, $S' = 1$ and consequently

$$\Delta\omega = -\pi N_e \int k^{-1} f(k) \sum_\ell (2\ell + 1) \sin 2\left(\tau_{p\ell} - \tau_{s\ell}\right) dk \ , \qquad (15)$$

where $\tau_{p\ell}$ and $\tau_{s\ell}$ are phase shifts associated with the scattering on the 2p and 1s levels, respectively. Furthermore,

$$\sin 2\left(\tau_{p\ell} - \tau_{s\ell}\right) = \sin 2\tau_{p\ell} - \sin 2\tau_{s\ell} + 4\sin\tau_{p\ell}\sin\tau_{s\ell}\sin\left(\tau_{p\ell} - \tau_{s\ell}\right) \ . \qquad (16)$$

The first two terms on the right-hand side of (16) correspond to the direct terms, and the third term to the interference term according to (2).

The importance of the interference term for $He^+$ is shown on Fig. 6 by curves J and K. J was obtained in the same way as A, but the interference term was not included. K similarly corresponds to C. It can be seen that the inclusion of upper levels and of exchange contributions significantly changes the magnitude of the interferenc term even if the total frequency shift is affected minimally.

Fig. 7 demonstrates the effect of exchange. Curves L, M, N, O were obtained by ignoring all exchange terms in the $\underset{\sim}{\rho}$ matrix. In addition, functions $F_{k\ell}$ with $\ell$=0,1 were not orthogonalized to bound wave functions. Curve L was obtained with all levels included. A comparison with A shows that the omission of exchange decreases

the total shift. Curve N represents pure elastic scattering, and it would be identical to C in Fig. 6 except for one thing: functions $F_{k\ell}$ used to calculate C were orthogonalized to bound wave functions, while those for N were not. The resulting difference is negligible. Curve M corresponds to L but without the interference term, and O similarly corresponds to N.

In Fig. 8, our result for ionized helium (A) is compared to the semi-classical calculation of Griem[3] and to the R-matrix method of Yamamoto and Narumi.[4]

The semi-classical result is about 35% lower than the DWX method at kT = 2.5 eV, but the agreement improves with higher temperature. However, there are basic differences between the semi-classical procedure and our method. The semi-classical result is derived solely from the second-order terms in the $\underset{\sim}{S}$ matrix elements, and in the expansion for the interaction potential only dipole and quadrupole terms have been taken into account. In the DWX method the main contribution to the shift comes from the monopole part of the potential and higher order contributions to the $\underset{\sim}{S}$ matrix are due to the unitarizing relation (10). The $\underset{\sim}{\rho}$ matrix has only first-order terms. Therefore a partial agreement between the two methods appears to be purely fortuitous. A more detailed comparison of both methods will be given in par. II.4.

The R-matrix calculation yields results which are almost three times smaller than the DWX approximation. Yamamoto and Narumi included in their calculation the same number of levels as we did (1s-3d), but there are several other differences which may cause the discrepancy. For example, they use the same basis set of functions for the scattering on both the upper and the lower state. According to Yamamoto[15], the potential for the scattering on $He^+$ was taken equal to (in our notation)

$$r^{-1}[1 + \exp(-2^{1/3}r)] \qquad (17)$$

as compared to our potential $2r^{-1} - V(r)$ with V(r) given by (7). In order to evaluate the effect of such a potential, we have repeated the calculations (including all levels up to 3d) using potential (17) to generate $F_{k\ell}$. Thus the differences of phase shifts $\tau_{p\ell} - \tau_{s\ell}$ disappear, but the diagonal elements $\rho(\alpha, \alpha)$ were supplemented by direct monopole terms which are missing in the DWX approximation according to (3) and which represent different elastic scattering on the upper and lower level. The result is shown as curve S on fig. 9 and it proves

that the form of the potential itself cannot explain the differences between our result and that of the R-matrix method. We suspect that the evaluation of elastic contributions in the R-matrix calculation is responsible for the discrepancy. We have performed two additional calculations to substantiate this suspicion: Curve T was obtained in the same way as S (i.e. using potential (17)), but without monopole terms in the $\underset{\sim}{\rho}$ matrix, and U corresponds to our original calculations (curve A), but with all phase shifts $\tau_{p\ell}$ set equal to $\tau_{s\ell}$ (the result is then independent on the actual value of $\tau_\alpha$). In both cases the effects of pure elastic scattering were removed from the calculation, and the agreement with Yamamoto and Narumi is much better, but still not satisfactory over the whole temperature range. A possible inadequacy of diagonal R-matrix elements in ref. 4 has already been pointed out by Griem.[3]

Observational evidence[5-8] concerning the Lyman-alpha shift in ionized helium is to a certain degree contradictory due to experimental difficulties. In contrast to our calculation which yields negative shifts, experimentally found shifts are positive (i.e. blue) and of much larger magnitude. At the present time it is not even clear if this discrepancy is caused by experimental inaccuracy or if it represents incompleteness of the theory.

For hydrogen (Figs. 10-12), the sensitivity of frequency shift to the inclusion of atomic levels in the $\underset{\sim}{S}$ matrix is much larger than for $He^+$.

The smallest shift is obtained with pure elastic scattering without exchange, i.e. with $\underset{\sim}{\rho} = 0$ (curve C, Fig. 10). The shift even reverses its sign and becomes blue at low temperature. The gap between A and C is much larger than for $He^+$. The largest shift is the result of inclusion of the 1s2s2p levels (curve D). Addition of the 3s and 3p levels (curve E, Fig. 11) decreases the shift and so does the inclusion of 3d (curve A). If 4d is included instead of 3d, the shift again becomes larger (G), therefore it is not possible to estimate simply the effect of levels with $n > 3$ by extrapolation. They may be important and, in contrast to ionized helium, their effect may not be negligible. Calculations without the interference term are represented by J and K (Fig. 10). J corresponds to A and K to C.

A comparison of results without exchange is displayed on Fig. 12. As in $He^+$, these results were obtained with no orthogonalization of $F_{k\ell}$ to bound wave functions. The omission of exchange and orthogonalization substantially increases the shift (L). Curve C (Fig. 10) and N (Fig. 12) representing results of pure elastic scattering differ only by orthogonalization of $F_{k\ell}$ with $\ell=0$ and 1 in curve C. For hydrogen this difference is substantial in contrast to $He^+$ and it is caused

entirely by an opposite sign of the partial contribution with $L_p$=1 in the DWX calculation (curve C). The effect arising by the omission of the interference term is indicated by M and O which correspond to L and N, respectively.

The semi-classical calculation of Griem[16] is compared to our DWX result (curve A) on Fig. 13. There is a discrepancy by a factor of five between the two calculations, and the disagreement appears to be due to the differences of both methods. A discussion of the discrepancy and a comparison with the experimental result will be given in par. II.4.

The contributions to the total frequency shift $\Delta\omega$ of the Lyman-alpha line of $He^+$ and hydrogen from angular momenta $L_p$ are shown on Figs. 14 and 15 for two values of temperature. In $He^+$, the major contribution corresponds to $L_p$=1, for higher angular momenta the contributions decrease monotonously. In hydrogen, the $L_p$=1 partial contribution is positive, while all others are negative. The opposite sign for $L_p$=1 is caused predominantly by orthogonality of $F_{k\ell}$ and $P(n\bar{\ell})$, and it is also the main source of difference between line A and L in Fig. 12.

## II.3. Shift of Lyman-alpha derived from electrostatic interaction.

Several authors have studied the Lyman-alpha shifts from the point of view of electrostatic interaction of the radiator and plasma.[11,17-19] Status of the theory prior to 1978 has been reviewed by Volonte'[17]. The basic assumption of this approach is that each atomic level is independently shifted by plasma interaction and that the frequency shift of the spectral line is equal to the difference of these level shifts. The level shifts are therefore derived without any regard to the radiative process from a static model of atom-plasma interaction.

It is easy to see the relationship between one particular form of "static line-shift" and formula (1). If all values $\tau_\alpha$ are small compared to unity and only pure elastic scattering significantly contributes to the line-shift, $\Delta\omega$ is given by (15) and $\sin2(\tau_{p\ell} - \tau_{s\ell})$ by (16) without the interference term. Assuming a spherical charge distribution of the atomic electron, we obtain from the perturbation expression for the phase shifts[20]

$$\sin2\left(\tau_{p\ell} - \tau_{s\ell}\right) \sim -4\int\left[V\left(n_p p;\ r\right) - V\left(n_s s;\ r\right)\right]\left[F^c_{k\ell}\ (r)\right]^2\ dr\ . \qquad (18)$$

Potentials $V(n\bar{\ell}; r)$ are defined by (7) and $F^c_{k\ell}$ are solutions of (6) with C=C'=0 and with $2(Z + 1)r^{-1} - 2V(n\bar{\ell}; r)$ replaced by $2Zr^{-1}$ (i.e. $F^c_{k\ell} = k^{1/2}r$ x spherical Bessel function for a neutral radiator or a Coulomb function for an ion). A spherically symmetric density distribution $n_e$ of mutually non-interacting free electrons moving in the field of a positive point charge Z with a momentum distribution f(k) can be written in the form

$$n_e(r) = N_e \int k^{-1} f(k) r^{-2} \sum_{\ell} (2\ell + 1) \left[F^c_{k\ell}(r)\right]^2 dk \qquad (19)$$

with $\lim_{r\to\infty} n_e = N_e$. The energy $W(n\bar{\ell})$ of electrostatic interaction of a bound electron in the $n\bar{\ell}$ state with free electrons described by (19) is

$$W(n\bar{\ell}) = 4\pi \int r^2 n_e(r) V(n\bar{\ell}; r) dr \ . \qquad (20)$$

The expression for $W(n\bar{\ell})$ diverges, but the difference $W(n\bar{\ell}) - W(n'\bar{\ell}')$ has a finite value.

Let us define a static frequency shift $\Delta\omega_{static}$ of the Lyman-alpha line as

$$\Delta\omega_{static} = W(2p) - W(1s) \ . \qquad (21)$$

Then, with respect to (18), the static shift (21) is identical to (15). It should be noted that for neutral radiators with Z=0, formula (19) represents a uniform density distribution.

It is convenient for the following discussion to denote by $\Delta\omega_{static\ I}$ the frequency shift (21) obtained from the uniform electron distribution, and by $\Delta\omega_{static\ II}$ the shift (21) if the functions $F^c_{k\ell}$ in (19) are Coulomb functions with $Z\neq 0$.

In the static shifts just described, the effect of the bound electron on the free electron density distribution has been ignored. This effect can be taken into account by replacing $F^c_{k\ell}$ in (20) by $F_{k\ell}$, which are solutions of (6) (with C=C'=0) and which are identical to the functions used in our distorted-wave approximation

without exchange. This procedure leads to another version of a static shift, and the result will be referred to as $\Delta\omega_{\text{static III}}$.

In a real physical situation, (18) is not always satisfied and the interference term is not negligible, so that the static shift may be substantially different from the shift calculated according to (1). Static shifts defined by (21) are compared with the DWX result (curve A) on Figs. 9 and 13 for $He^+$ and hydrogen, respectively.

For ionized helium, $\Delta\omega_{\text{static I}}$ (curve R) is much smaller than $\Delta\omega_{\text{static II}}$ (Q) and $\Delta\omega_{\text{static III}}$ (P). The difference is obviously caused by a much weaker interaction of the bound electron with uniform electron background that with electrons attracted to the radiator by the ion field. A relatively good agreement of P and A is probably a pure coincidence. On the other hand, the agreement of $\Delta\omega_{\text{static II}}$ (curve Q) with the distorted-wave calculation without exchange and without inelastic terms (curve O) is rather poor in spite of the fact that both results were derived from the same expression (15). This indicates the inadequacy of (18) for the replacement of phase shifts by perturbation expression.

In hydrogen (Fig. 13), A is much smaller than $\Delta\omega_{\text{static I}}$ (R) and $\Delta\omega_{\text{static III}}$ (P). The phase shifts $\tau_\alpha$ for hydrogen scattering are not small and therefore (18) cannot be valid.

## II.4. Comparison of the semi-classical calculation and the DWX method.

On Figs. 8 and 13, the results of the semi-classical (SC) calculations[3,16] (circles) for the Lyman-alpha shift are compared to the values obtained from the present DWX method (curve A). There is a large discrepancy between the two results for hydrogen, while for $He^+$ the agreement is much better, although not satisfactory.

In the semi-classical calculation, the first-order contributions to the line shift vanish, and the shift is obtained from the second-order terms in the expansion for the $\underset{\sim}{S}$ matrix elements. The second-order terms do not contain any monopole contributions. Moreover, the interference term in the expression (2) is ignored, and the line shift is equal to the difference of level shifts. The dipole contribution to the shift of an $n\bar{\ell}$ level from electrons with velocity v and impact parameter $\rho_i$ is proportional to[3,16]

$$(\rho_i\ v)^{-1} \sum_{n'\bar{\ell}'} \max(\bar{\ell}',\ \bar{\ell})\ |\langle n'\bar{\ell}'|r|n\bar{\ell}\rangle|^2\ B\ , \tag{22}$$

where $n'\bar{\ell}'$ are all possible final states produced by collisions of electrons with the radiator in the state $n\bar{\ell}$, and B is the shift function depending on $\rho_i$, v, and $E_{n\bar{\ell}} - E_{n'\bar{\ell}'}$. Quadrupole contributions, which are much less important, are proportional to a similar expression, and they involve matrix elements $\langle n'\bar{\ell}'|r^2|n\bar{\ell}\rangle$.

In the present DWX approximation, the matrix elements $\rho(\alpha,\ \alpha)$ and $S(\alpha,\ \alpha)$ are calculated from the first-order perturbation theory and contain no contributions of type (22). In order to obtain second-order contributions, one has either to solve coupled equations for the scattering problem or to employ the second-order perturbation theory. In the following we use a simplified form of the latter procedure.

Expression (3) for the elements of the $\underline{\rho}$ matrix may be obtained from the Kohn's variational principle

$$\rho(\alpha,\ \alpha') = -2 \sum_{\text{spins}} \int \Psi^*_{\alpha'}\ (H - E)\ \Psi_\alpha\ d\vec{r}_1 d\vec{r}_2\ , \tag{23}$$

where $\Psi_\alpha$ and $\Psi_{\alpha'}$ are trial wave functions of the total system (including spin) corresponding to the channel $\alpha$ and $\alpha'$, respectively. $\Psi_\alpha$ has the form (for simplicity we use here unsymmetrized functions)

$$\Psi_\alpha = Q_\alpha\ r_2^{-1}\ F_{k_\alpha \ell_\alpha}\left(r_2\right) \tag{24}$$

with

$$Q_\alpha = \sum_{\substack{\bar{m}\ \bar{m}_s \\ m\ m_s}} C^{\bar{\ell}_\alpha\ \ell_\alpha\ L_T^T}_{\bar{m}\quad m\quad M_L}\ C^{1/2\ \ 1/2\ \ S^T}_{\bar{m}_s\quad m_s\quad M_S}\ \bar{\Phi}\left(\bar{\ell}_\alpha\ \bar{m}\ \bar{m}_s\right)\ r_1^{-1}\ P\left(n_\alpha\ \bar{\ell}_\alpha;\ r_1\right)\ \Phi\left(\ell_\alpha\ m_\alpha\ m_s\right), \tag{25}$$

where all symbols with bars refer to the bound electron, $\bar{\Phi} r_1^{-1} P$ is the wave function of the bound electron including spin, and $\Phi$ is the angular and spin part of the function for the colliding electron. Improved values of diagonal elements $\rho(\alpha, \alpha)$ may be obtained if the trial function $\Psi_\alpha$ in (23) is replaced by a corrected function $\Psi_\alpha^{corr}$ which also contains terms representing scattering, so that

$$\Psi_\alpha^{corr} = Q_\alpha r_2^{-1} F_{k_\alpha \ell_\alpha}(r_2) + \sum_{\alpha' \neq \alpha} Q_{\alpha'} r_2^{-1} G_{k_{\alpha'} \ell_{\alpha'}}(r_2) \quad . \tag{26}$$

The asymptotic form of G should be

$$G_{k_{\alpha'} \ell_{\alpha'}}(r) \sim \rho(\alpha, \alpha') k_{\alpha'}^{-1/2} \cos\left[k_{\alpha'} r - \frac{1}{2} \ell_{\alpha'} \pi + Z k_{\alpha'}^{-1} \ell n(2 k_{\alpha'} r)\right.$$

$$\left. + \arg \Gamma\left(\ell_{\alpha'} + 1 - i Z k_{\alpha'}^{-1}\right) + \tau_{\alpha'}\right] \quad .$$

In our simplified procedure we replace $G_{k_{\alpha'} \ell_{\alpha'}}$ by $\rho(\alpha, \alpha') F_{k_{\alpha'} \ell_{\alpha'}}$ which has the same amplitude at infinity, but has an incorrect phase. Therefore the values of matrix elements (23) will be subject to errors which may be difficult to estimate. However, with this replacement, (23) assumes a very simple form, and the resulting expression for the second-order contributions to the level shift contains terms of the type (22) and is therefore directly comparable to the SC formula. Assuming that elements $\rho(\alpha, \alpha')$ are small and retaining only terms up to the second order in $\rho(\alpha, \alpha')$, we obtain from (23) for the corrected diagonal matrix element

$$\rho^{corr}(\alpha, \alpha) = \rho(\alpha, \alpha) + 2 \sum_{\alpha' \neq \alpha} \rho^2(\alpha, \alpha') \quad . \tag{27}$$

The same result is obtained if one uses antisymmetric function $\Psi_\alpha$ and (27) is therefore generally valid.

On Figs. 16 and 18 we compare our previous result (curve A) with line shift obtained from matrix elements $\rho^{corr}(\alpha, \alpha)$ according to (27).

For $He^+$ (Fig. 16), the result of inclusion of all second-order terms for angular momenta up to $L^T=13$ is represented by curve $B_1$. However, the sum over all $L^T$ is divergent due to the contributions from the 2p-2s transition with $\Delta E=0$. If the second-order terms due to this transition are excluded, the shift is given by curve $A_1$. The effect of the 2p-2s transition cannot be properly treated without consideration of plasma effects on electron collisions, because contributions from distant collisions corresponding to large angular momenta $L^T$ are substantially reduced due to plasma screening effects. In a recent paper, Griem[21] has obtained values of contributions to the Lyman-alpha shift from $\Delta n=0$ transitions for $He^+$ and H for the electron density $N_e=10^{17}$ $cm^{-3}$ following the method of Boercker and Iglesias.[22] If we add these contributions to the values given by curve $A_1$ (scaled to $N_e=1$ for the sake of comparison), we obtain the final result for the Lyman-alpha shift represented by curve $C_1$.

The inclusion of second-order terms into our DWX method makes the disagreement between the Griem's original SC calculation[3] (Figs. 8 and 17) and our present results even greater. In the semi-classical calculation, the main contributions to the shift originate from the 2p-3s and 2p-3d transitions, but the total effect of the second-order inelastic term in the DWX approximation (difference of curves A and $A_1$ on Fig. 16) is much smaller than the total SC shift (Fig. 17). In order to find out if the discrepancy is just a result of differences inherent to both methods, we have performed a quantum-mechanical calculation which follows closely many features of a SC procedure: we have used a unitarized Coulomb-Bethe approximation with inclusion of second-order terms according to (27), but we have taken into account only contributions from the 2p-3s and 2p-3d transitions. The result is represented by curve $D_1$ on Fig. 17. If our results are extrapolated to kT=5 eV, the agreement with the SC calculation is good. The disagreement at low temperature may be caused by the fact that in the SC procedure the integration over the velocity distribution includes also non-vanishing contributions from energies below the inelastic threshold. To estimate the affect of such contributions, we repeated the previous calculation and set the values of all matrix elements below the n=3 threshold equal to their corresponding threshold values, thus obtaining an upper limit for the shift. The result is shown as curve $E_1$ on Fig. 17, and it demonstrates the drastic effect of contributions from energies below the threshold. From the results for $He^+$ shown on Figs. 16 and 17 we conclude that the difference of line shifts obtained from the DWX method and from the SC calculation is caused by several effects: elastic monopole contributions which represent a dominant part of the DWX shift are not taken into account in the SC procedure. On the other

hand, the inelastic second-order dipole terms are much larger in the SC method than in the DWX approximation (agreement with the Coulomb-Bethe approximation is much better), and contributions from energies below the inelastic threshold further increase the line shift in the SC calculation, while these contributions are ignored in the DWX calculation. Several other details of the semi-classical calculation may also contribute to the discrepancy. E.g., the method of unitarization (eq. 9 of ref. 3) makes some allowance for higher-order perturbation theory terms. In the DW method, the unitarization is achieved by a different procedure (eq. 10).

Turning to hydrogen (Fig. 18), we find that the effect of second-order terms in the DWX approximation is greater than in $He^+$ (curves $B_1$ and $A_1$). Supplementing results shown as $A_1$ by contributions due to $\Delta n=0$ transitions given by Griem[21] and scaled to $N_e=1$, we obtain curve $C_1$ which is in a good agreement with the experimental value of Gruetzmacher and Wende[23], from which the ion quadrupole contribution according to Griem[16] has been subtracted. (The result of ref. 23 should be taken with caution, however, because of uncertainties caused by the J-splitting and by the fact that the measured width is greater than the shift.) As in $He^+$, second-order inelastic contributions in the DWX approximation (difference of curves A and $A_1$ on Fig. 18) are smaller than the total shift from the SC calculation (Fig. 13). On Fig. 19 we again compare results of a unitarized Bethe approximation (with the inclusion of second-order terms and contributions limited to 2p-3s and 2p-3d transitions) and semi-classical shifts from $\Delta n=1$ transitions[16] (circles). In the SC calculation, the contributions to the shift from energies below the n=3 threshold do not vanish. These contributions represent the effects of resonances in the elastic scattering which are ignored in the DWX and Bethe approximations. If the contributions from energies below the inelastic threshold are excluded in the SC calculation, one obtains results shown as triangles in Fig. 19. However, this result still corresponds to a finite value of excitation cross section at threshold, and consequently it has to be larger than the result of the Bethe approximation. Figs. 18 and 19 for hydrogen therefore lead to a conclusion similar to that reached for $He^+$, and large values of SC shifts in comparison to the DWX results are caused mainly by larger second-order terms and by non-vanishing contributions from energies below and in the vicinity of the n=3 threshold.

## III. Summary of conclusions.

Frequency shifts of the Lyman-alpha line for ionized helium and hydrogen calculated in the DWX approximation are negative. The main contributions to the line shift are due to elastic scattering on the 2p level, but the shift is substantially affected by the inclusion of inelastic terms in the scattering matrix, and the effect is larger in H than in $He^+$. In hydrogen, contributions from levels higher than 3d (not included in the present calculation) may not be negligible. Second-order terms in the scattering matrix, representing coupling of different channels, are very important.

The interference term increases the absolute value of the line shift, and the effect is larger for H than for $He^+$.

Major contributions to the shift come from the lowest angular momenta of the colliding electrons.

The static shift of the line, defined as a difference of electrostatic interactions of the bound electron with plasma electrons moving in the potential of a point charge Z, is larger than the shift from the DWX method, but the agreement for $He^+$ is much better than for hydrogen.

The present DWX results for the shift of ionized helium are almost three times larger than results of the R-matrix method by Yamamoto and Narumi[4]. A possible explanation is the difference of elastic terms in both methods.

The difference of the DWX results and the semi-classical calculations of Griem[3,16] is attributable to several effects: elastic monopole contributions that represent a major part of the DWX shift are not included in the SC calculations; inelastic second-order terms are much larger in the SC method than in the DWX approximation; and inelastic contributions from energies below the n=3 threshold representing resonance effects in elastic scattering, were not taken into account in the DWX method.

Experimentally found positive shifts of the Lyman-alpha line of $He^{+5-8}$ are in sharp contrast to our calculation which yields negative shifts of much smaller magnitude. Observed electron collision shift of the Lyman-alpha line of hydrogen is in agreement with the DWX result, if second-order terms are included and contributions due to the 2p-2s transition according to Griem[21] are taken into account.

With respect to previous discussions, the most reliable result of the present investigation (combined with partial result of Griem[21] for contributions due to the 2p-2s transition) is represented by curves $C_1$ on Figs. 16 and 18. It applies, however, only to electron density $N_e \approx 10^{17}$ $cm^{-3}$ for which the results of ref. 21 have been obtained. Further improvement in future calculations should be

accomplished by properly taking into account second-order terms in the scattering matrix either by using close-coupling results or by rigorously applying the second-order perturbation theory, and by taking into account the effect of resonances below inelastic thresholds.

## Acknowledgements

This work was supported by the Office of Naval Research.

The authors are indebted to Prof. Hans R. Griem for valuable discussions and comments.

## References

1. H.F. Berg, A.W. Ali, R. Lincke, and H.R. Griem, Phys. Rev. 125, 199 (1962).
2. M. Baranger, Phys. Rev. 111, 481 (1958).
3. H.R. Griem, Phys. Rev. A 27, 2566 (1983).
4. K. Yamamoto and H. Narumi, Progr. Theor. Physics 64, 436 (1980).
5. J.R. Greig, H.R. Griem, L.A. Jones, and T. Oda, Phys. Rev. Lett. 24, 3 (1970).
6. A.H. Gabriel and S. Volonté, J. Phys. B:Atom. Molec. Phys. 6, 2684 (1973).
7. T. Goto and D.D. Burgess, J. Phys. B:Atom. Molec. Phys. 7, 857 (1974).
8. M. Neiger and H.R. Griem, Phys. Rev. A 14, 291 (1976).
9. O. Theimer and P.C. Kepple, Phys. Rev. A 1, 957 (1970).
10. S. Volonté, J. Phys. B:Atom. Molec. Phys. 8, 1170 (1975).
11. R. Cauble, J. Quant. Spectrosc. Rad. Transfer 28, 41 (1982).
12. H.E. Saraph, M.J. Seaton, and J. Shemming, Phil. Trans. Roy. Soc. London A 264, 77 (1969).
13. I.C. Percival and M.J. Seaton, Proc. Camb. Phil. Soc. 53, 654 (1957).
14. D.H. Oza, Phys. Rev. A 33, 824 (1986).
15. K. Yamamoto, J. Phys. Soc. Japan, 49, 730 (1980).
16. H.R. Griem, Phys. Rev. A 28, 1596 (1983).
17. S. Volonté, J. Phys. D:Appl. Phys. 11, 1615 (1978).
18. J.C. Adcock and H.R. Griem, Phys. Rev. Lett. 50, 1369 (1983).
19. J. Davis and M. Blaha, J. Quant. Spectrosc. Rad. Transfer 27, 307 (1982).
20. N.F. Mott and H.S.W. Massey, The Theory of Atomic Collisions, Oxford Univ. Press (1965).
21. H.R. Griem, to be published in Phys. Rev. (1988).

22. D.B. Boercker and C.A. Iglesias, Phys. Rev. A 30, 2771 (1984).
23. K. Gruetzmacher and B. Wende, Spectral Line Shapes 4, 58 (1987).

Table 1

Results for the Lyman-alpha shifts shown on Figs. 6-13.

(DWX = distorted-wave approximation with exchange
DW = distorted-wave approximation without exchange)

| Curve | Levels included in the scattering matrix | Remark |
|---|---|---|
| A | 1s2s2p3s3p3d | DWX |
| B | 1s2p | DWX |
| C | 1s2p | DW, only elastic terms included, $F_{k\ell}$ orthogonalized to $P(n\bar{\ell})$ with $\ell=\bar{\ell}$ |
| D | 1s2s2p | DWX |
| E | 1s2s2p3s3p | DWX |
| G | 1s2s2p3s3p4d | DWX |
| J | 1s2s2p3s3p3d | DWX, same as A without interference term |
| K | 1s2p | DW, same as C without interference term |
| L | 1s2s2p3s3p3d | DW |
| M | 1s2s2p3s3p3d | DW, same as L without interference term |
| N | 1s2p | DW, only elastic terms included, $F_{k\ell}$ not orthogonalized to $P(n\bar{\ell})$ |
| O | 1s2p | DW, same as N without interference term |
| S | 1s2s2p3s3p3d | DWX, $F_{k\ell}$ generated using Yamamoto and Narumi's[4,15] potential |
| T | 1s2s2p3s3p3d | DWX, same as S, without direct monopole terms |
| U | 1s2s2p3s3p3d | DWX, same as A, with all $\tau_{p\ell}=\tau_{s\ell}$ |
| P | - | static shift $\Delta\omega_{\text{static III}}$ (from distorted waves $F_{k\ell}$) |
| Q | - | static shift $\Delta\omega_{\text{static II}}$ (from Coulomb functions $F^{c}_{k\ell}$ |
| R | - | static shift $\Delta\omega_{\text{static I}}$ (from uniform electron background) |

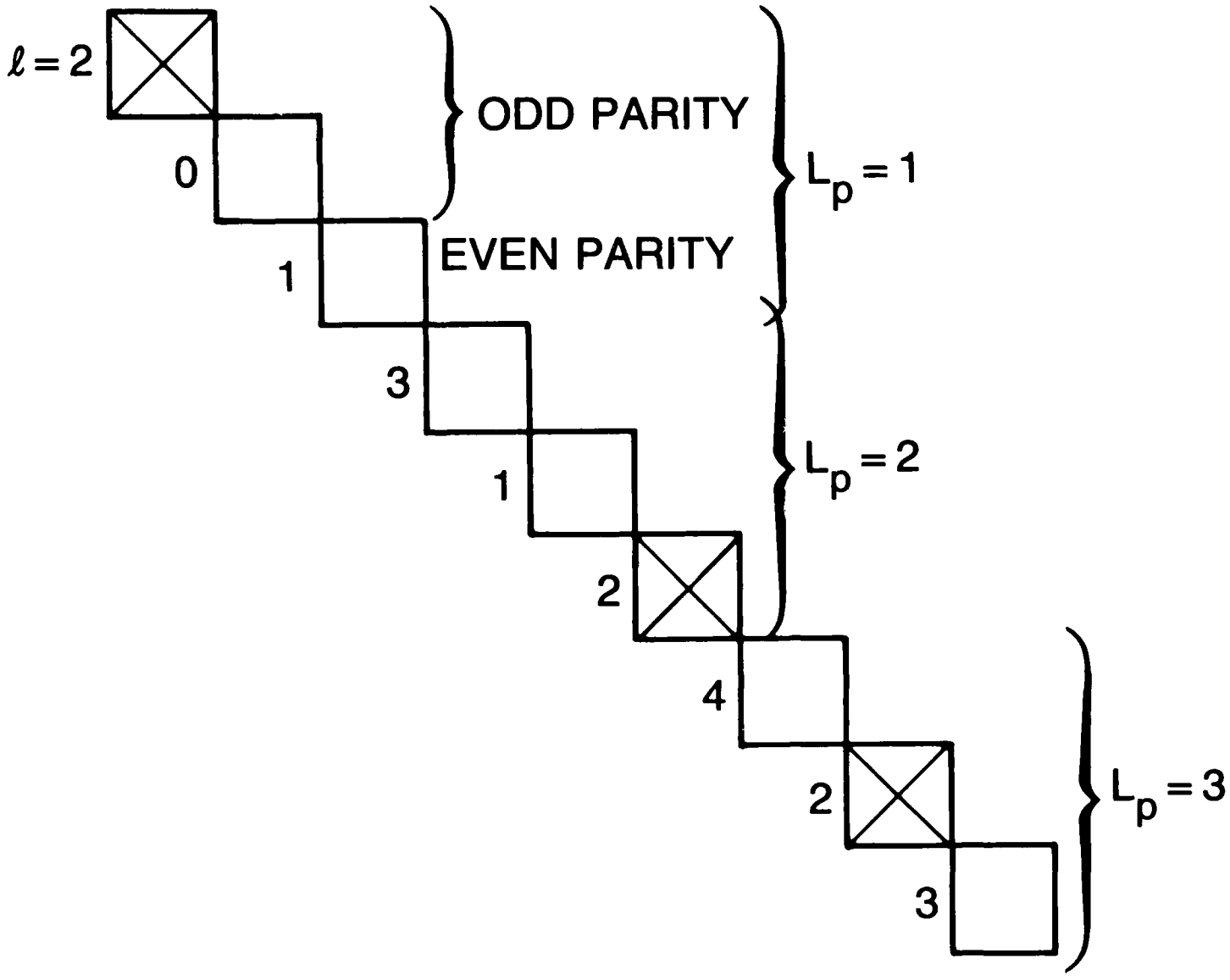


Fig. 1. Diagonal matrix elements $S(\alpha_p, \alpha_p)$ with $L_p$=1,2,3. Elements corresponding to $\ell$=2 are marked by X.

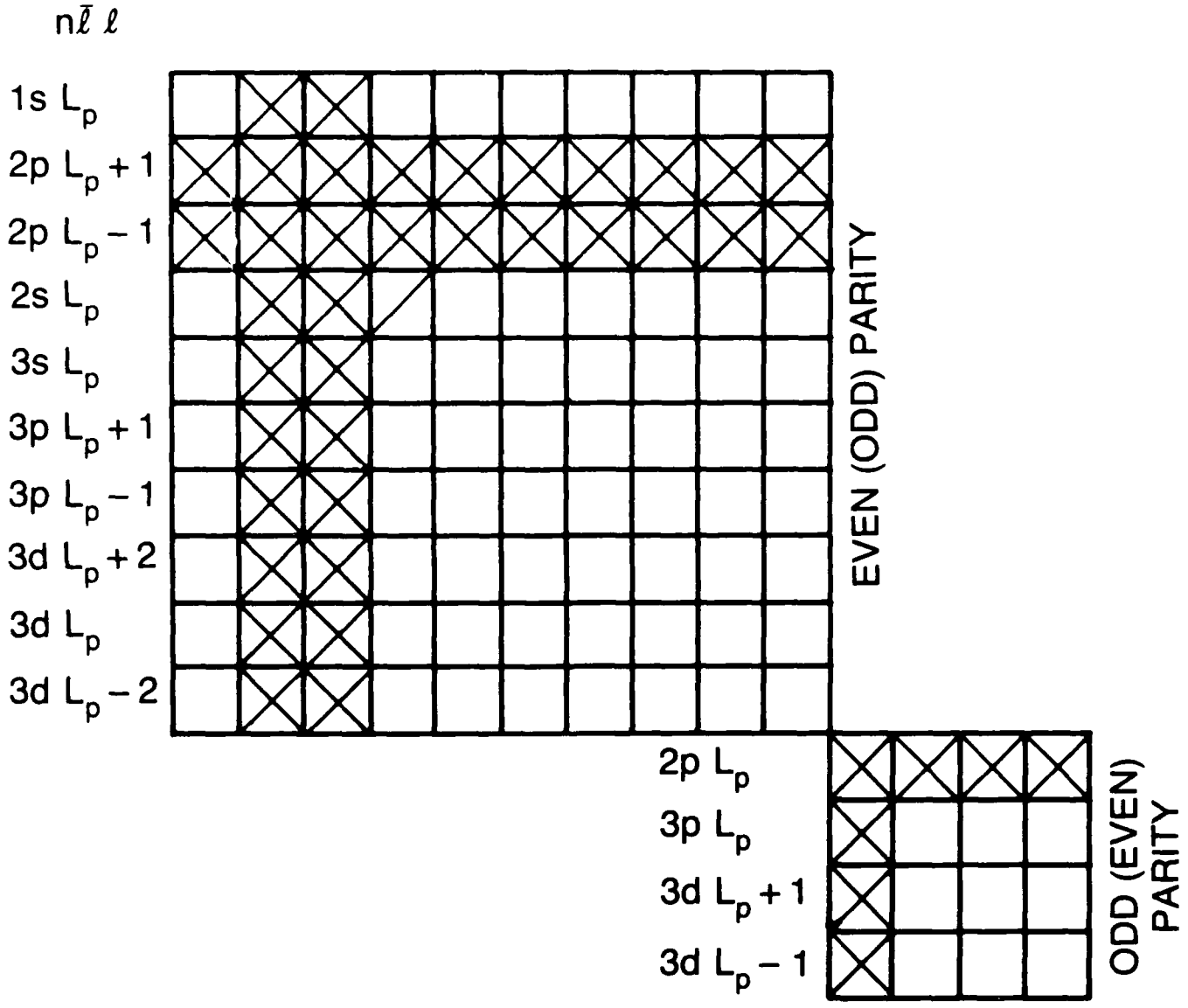


Fig. 2. Transmission matrix $\underset{\sim}{T}$ (for one set of values $L_p$, $S^T$) used for the calculation of diagonal elements $T(\alpha_p, \alpha_p)$. Elements included in the present calculation are marked by X.

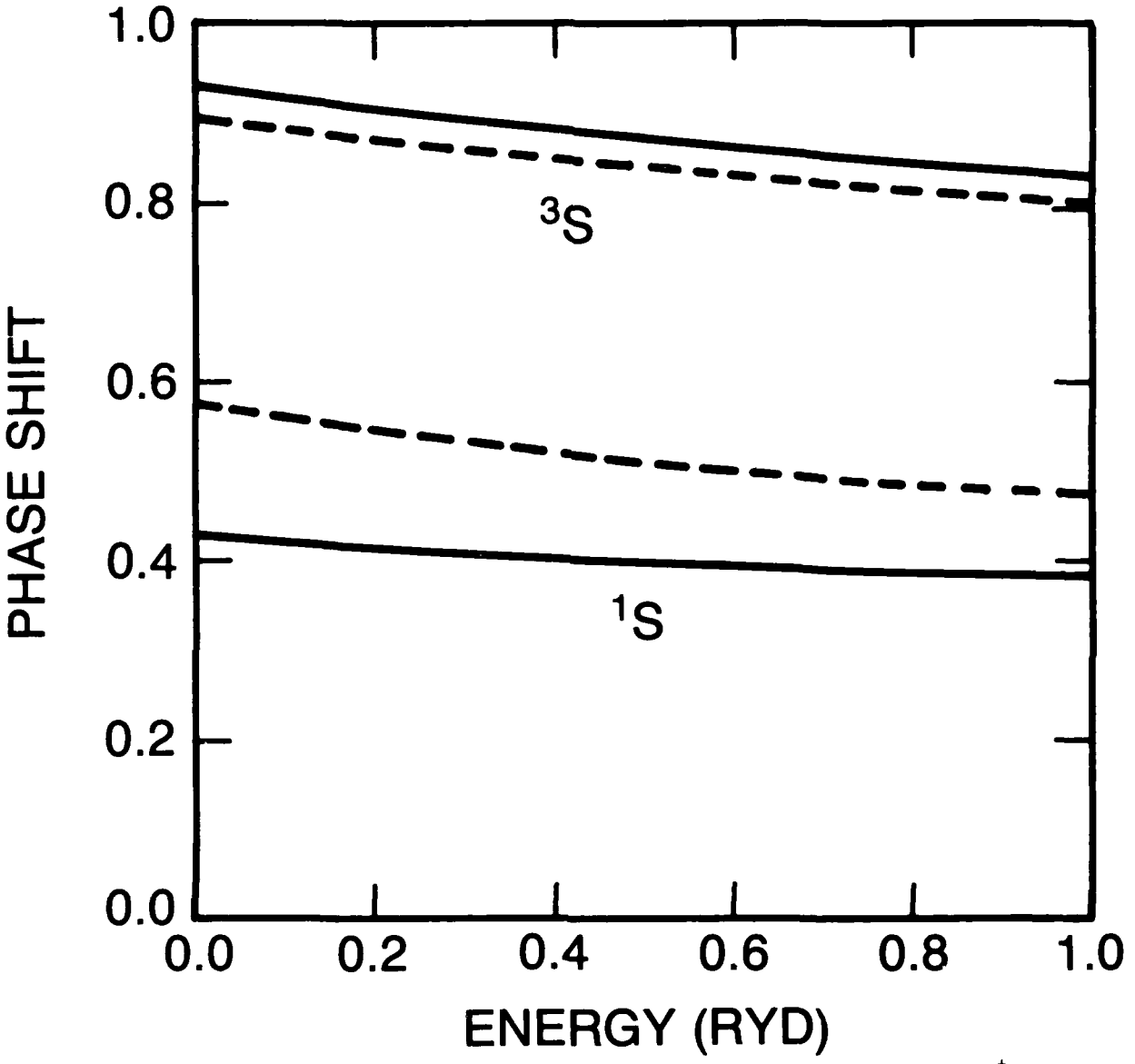


Fig. 3. S-phase shift (radians) for scattering on the 1s state of $He^+$. Solid curve: pseudo-state close-coupling calculation by Oza[14]; dashed curve: present result from the DWX approximation, eq. (14).

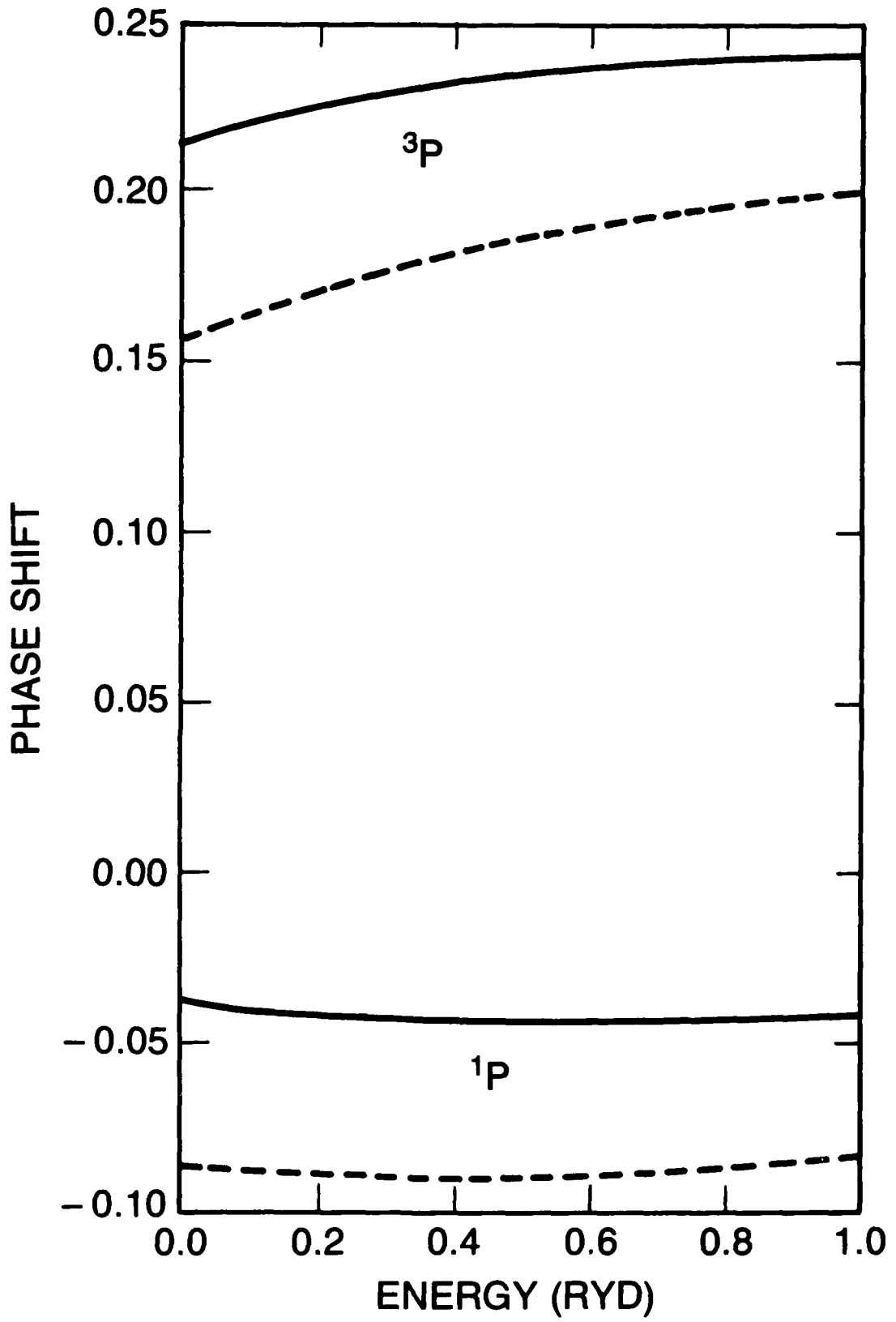


Fig. 4. P-phase shift (radians) for scattering on the 1s state of $He^+$. Solid curve: Oza[14]; dashed curve: eq. (14).

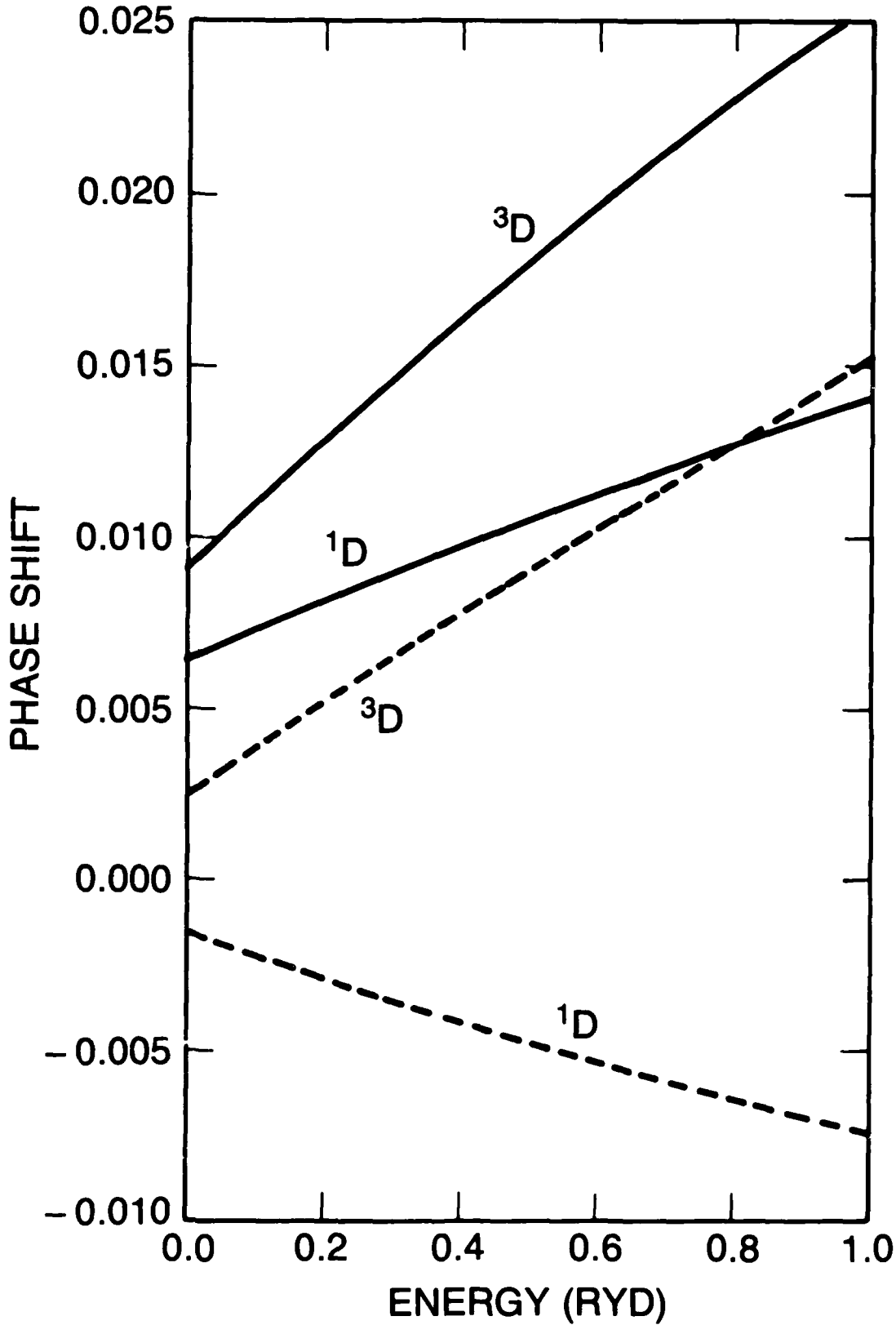


Fig. 5. D-phase shift (radians) for scattering on the 1s state of $He^+$. Solid curve: Oza[14]; dashed curve: eq. (14).

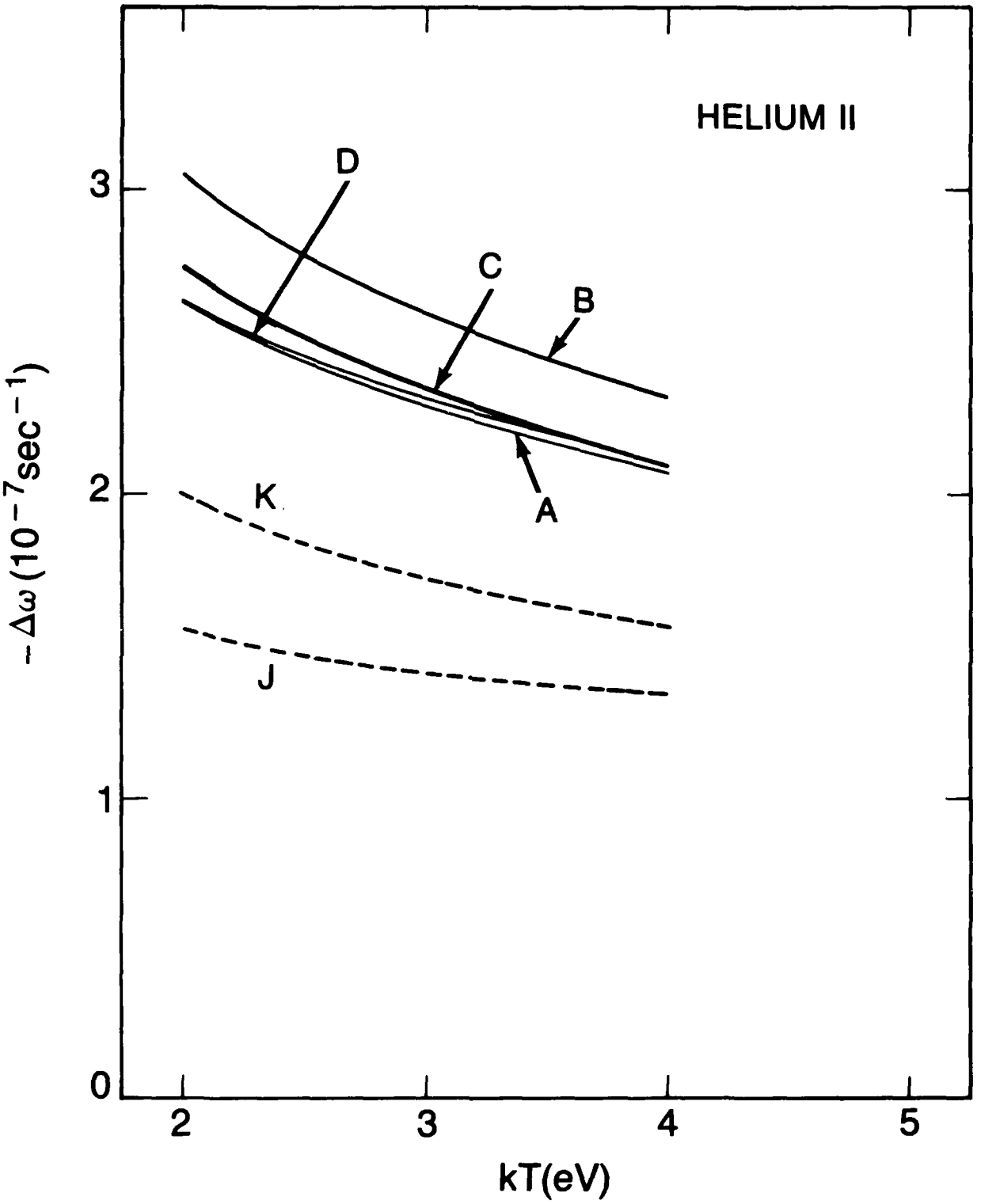


Fig. 6. Lyman-alpha shift of $He^+$. Symbols are explained in Table 1.

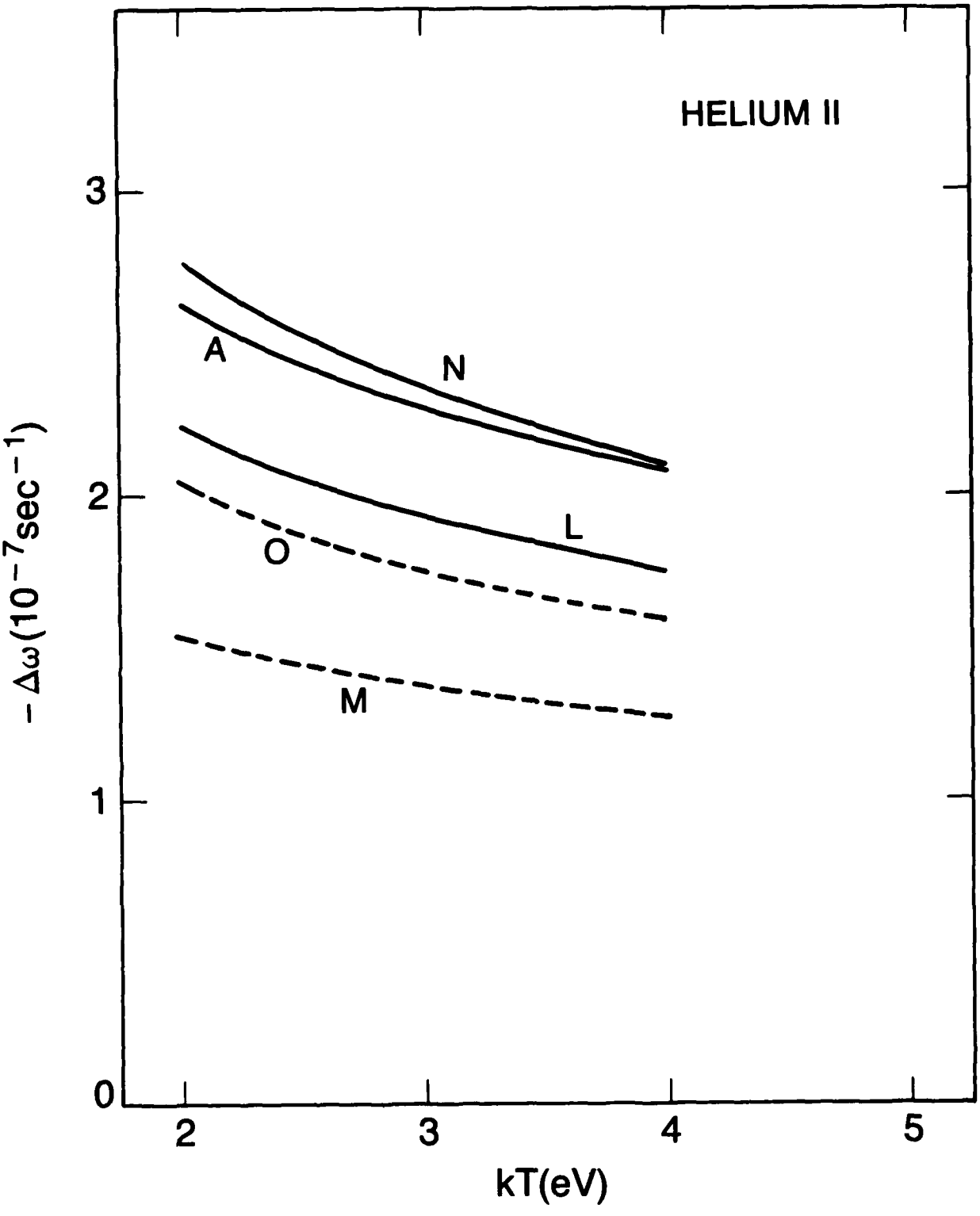


Fig. 7. Lyman-alpha shift of $He^+$. Symbols are explained in Table 1.

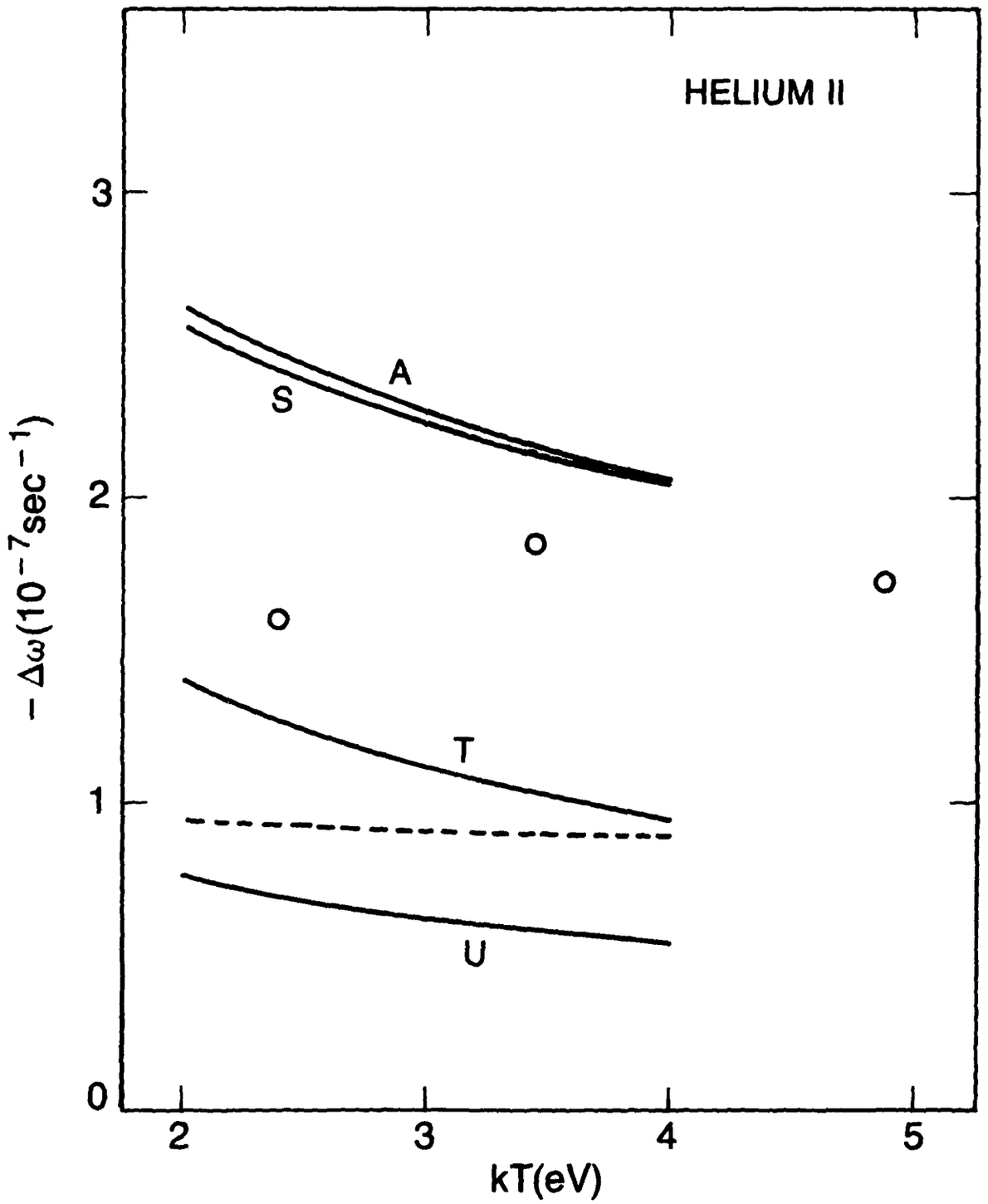


Fig. 8. Lyman-alpha shift of $He^+$. Symbols are explained in Table 1. Cirles: semi-classical calculation of Griem[3]; dashed line: R-matrix method of Yamamoto and Narumi[4].

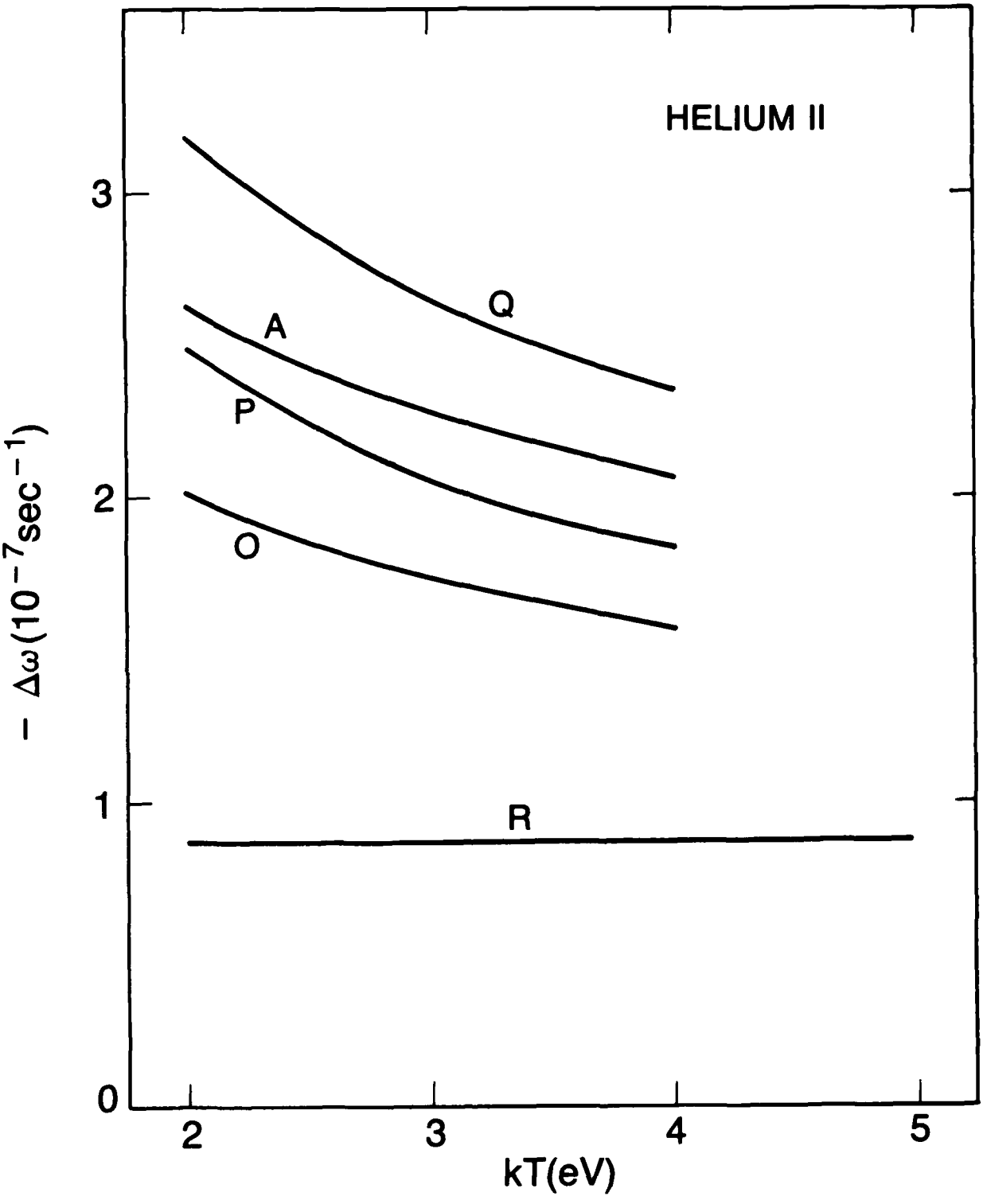


Fig. 9. Lyman-alpha shift of $He^+$. Symbols are explained in Table 1.

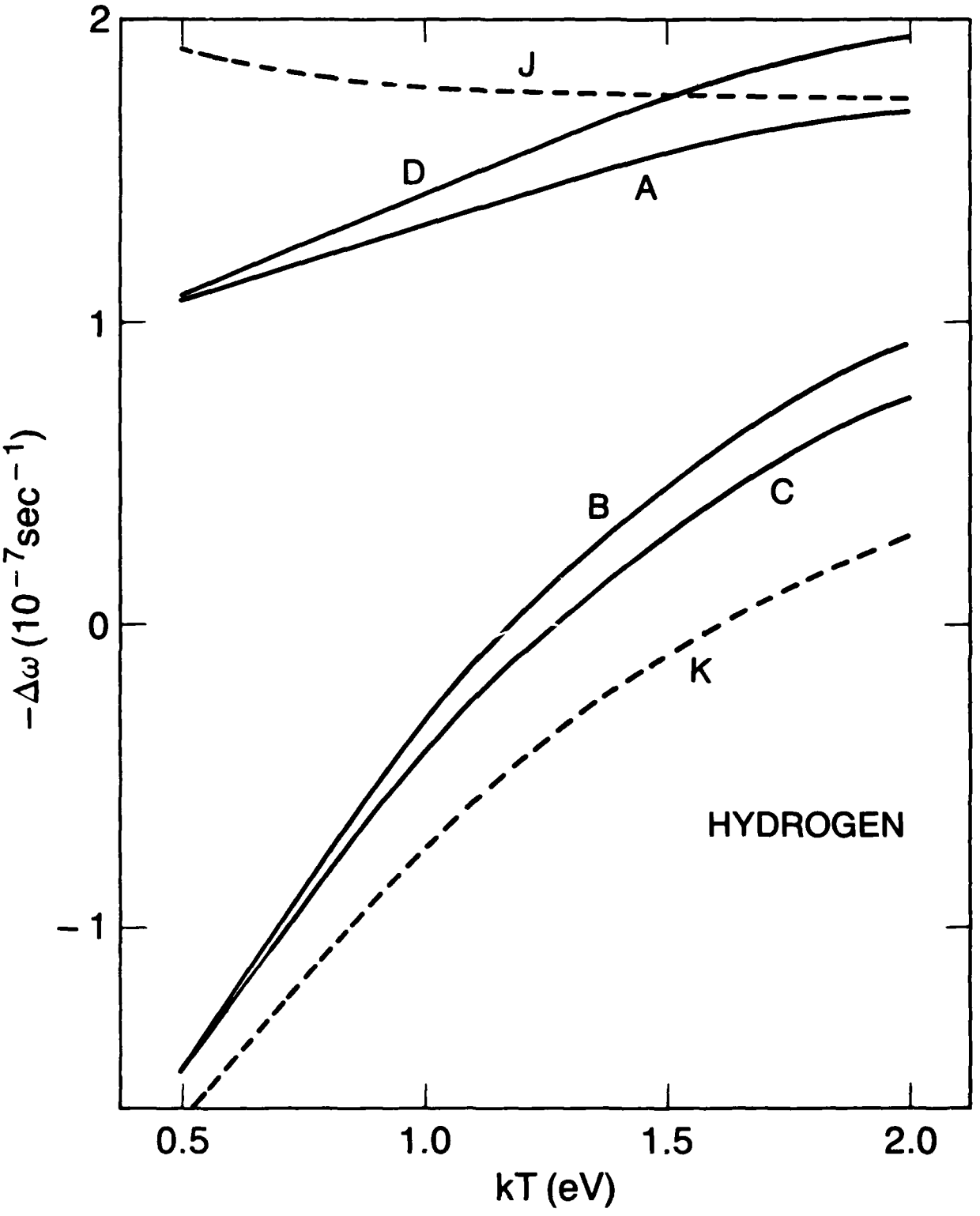


Fig. 10. Lyman-alpha shift of hydrogen. Symbols are explained in Table 1.

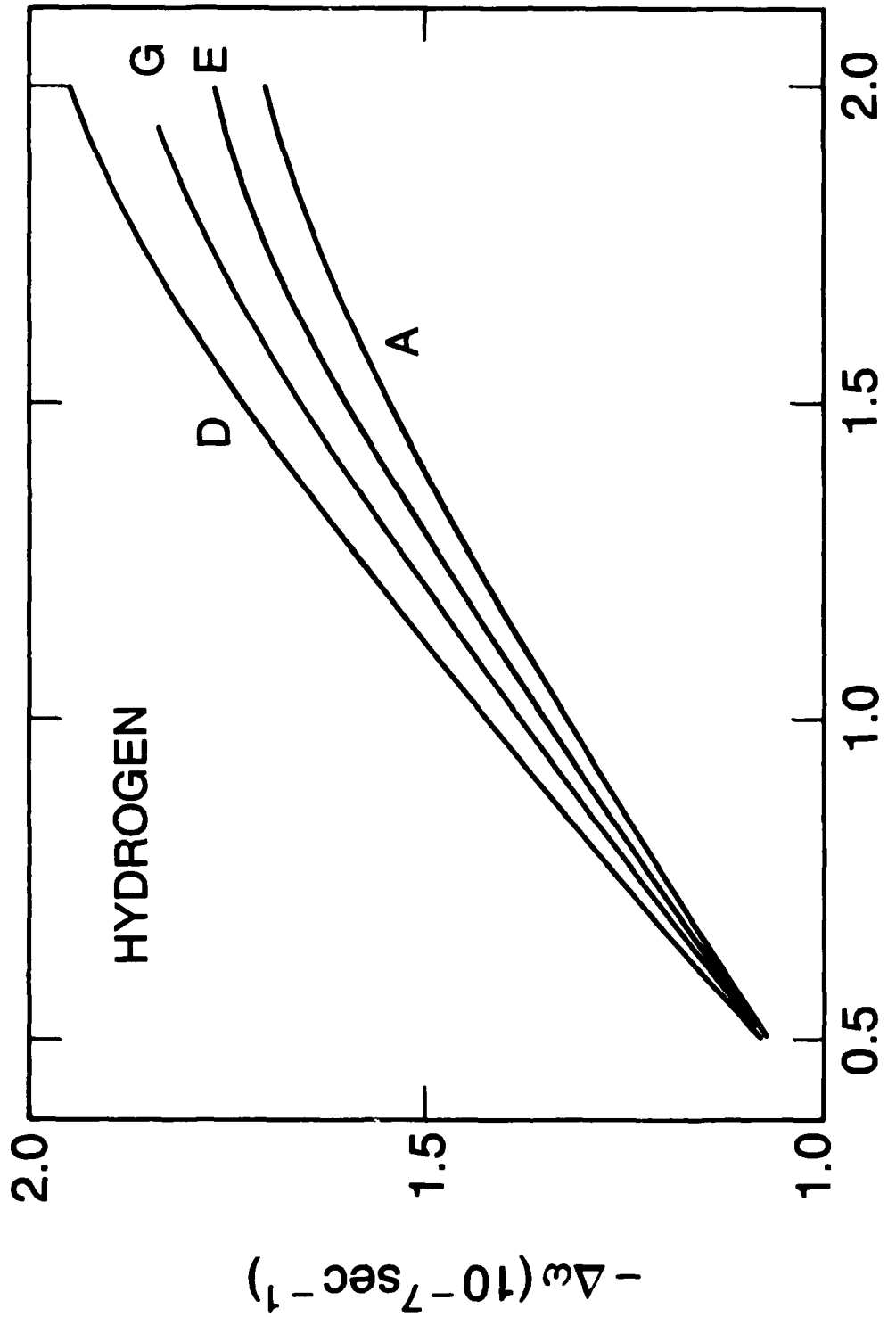


Fig. 11. Lyman-alpha shift of hydrogen. Symbols are explained in Table 1.

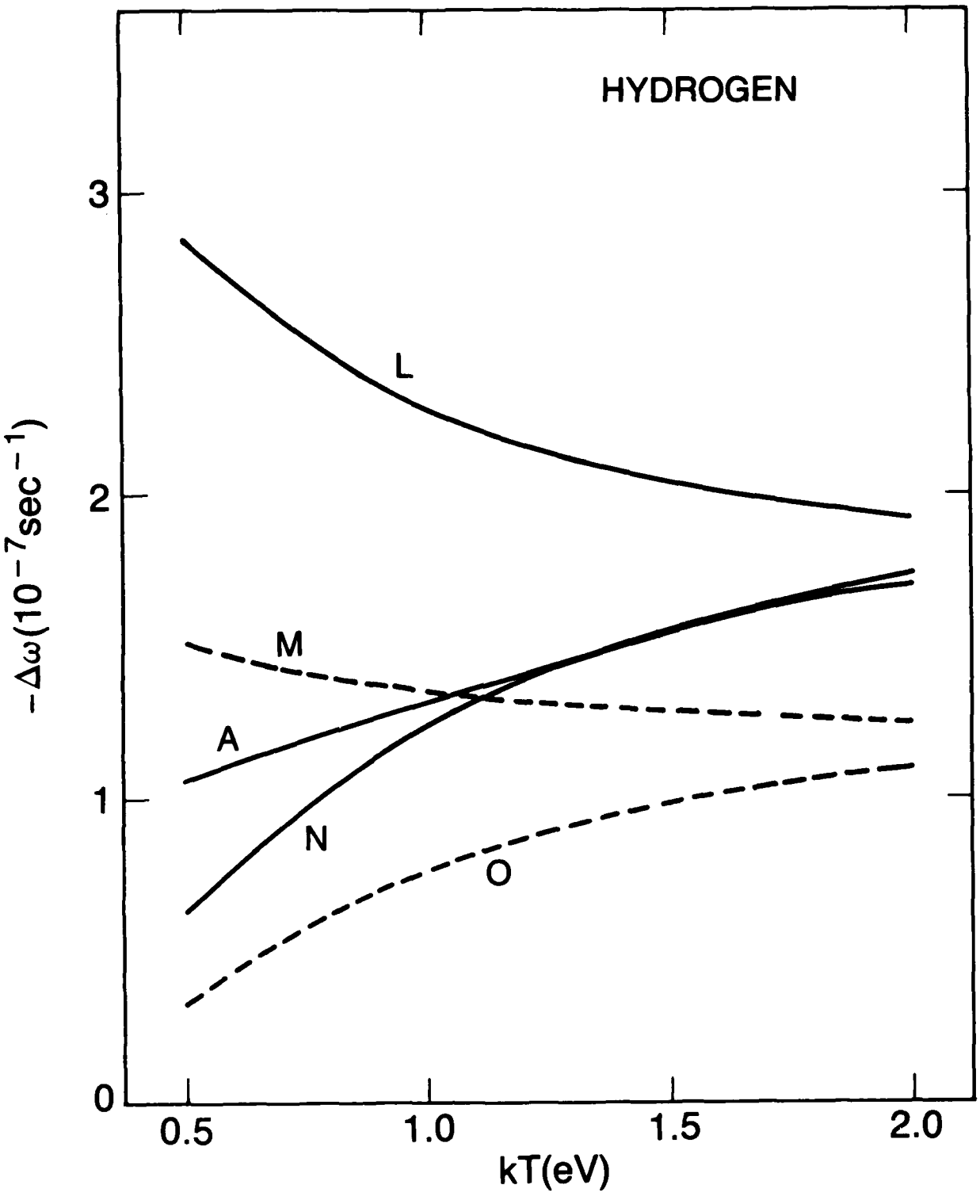


Fig. 12. Lyman-alpha shift of hydrogen. Symbols are explained in Table 1.

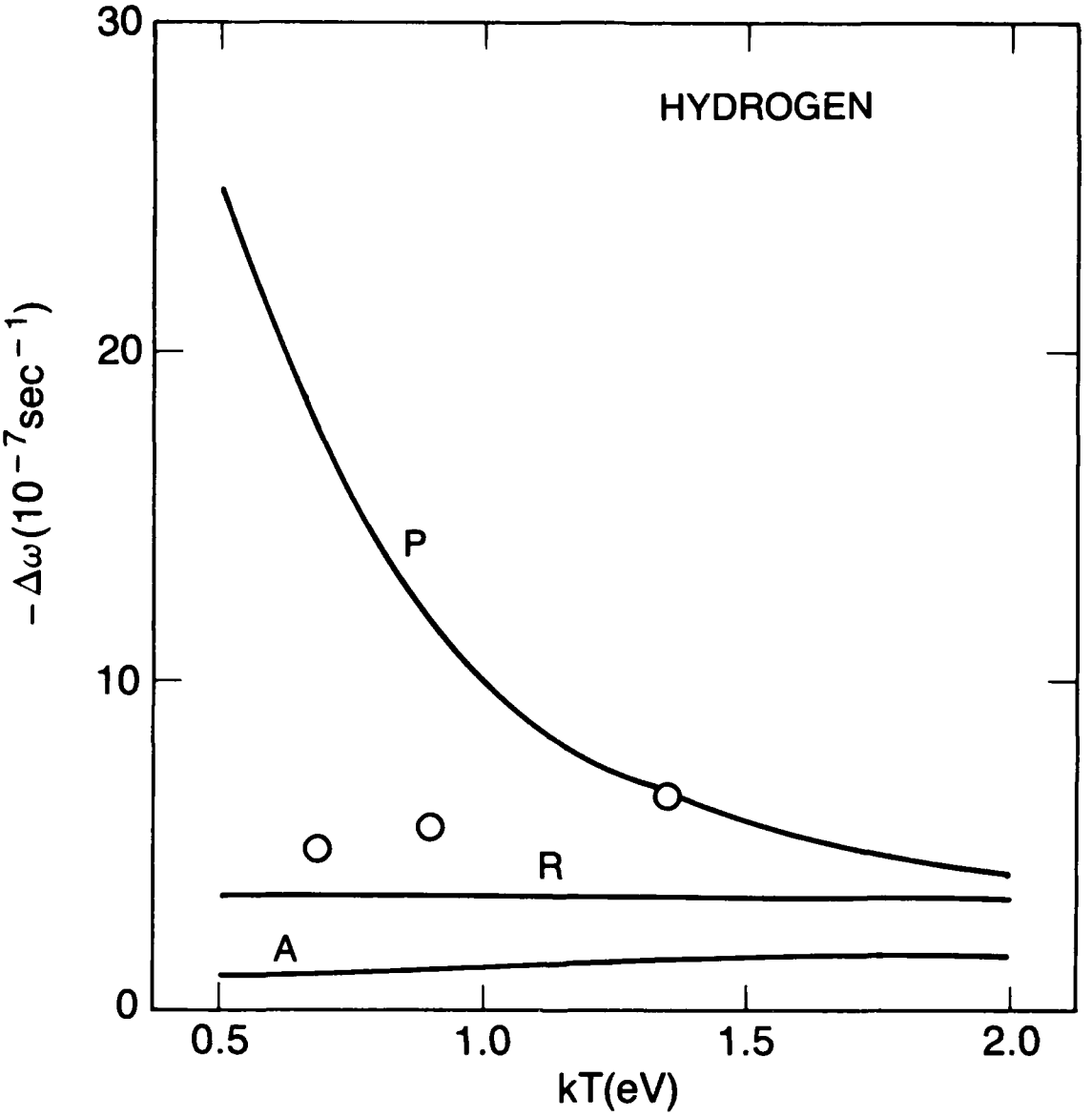


Fig. 13. Lyman-alpha shift of hydrogen. Symbols are explained in Table 1. Circles: semi-classical calculation of Griem[16].

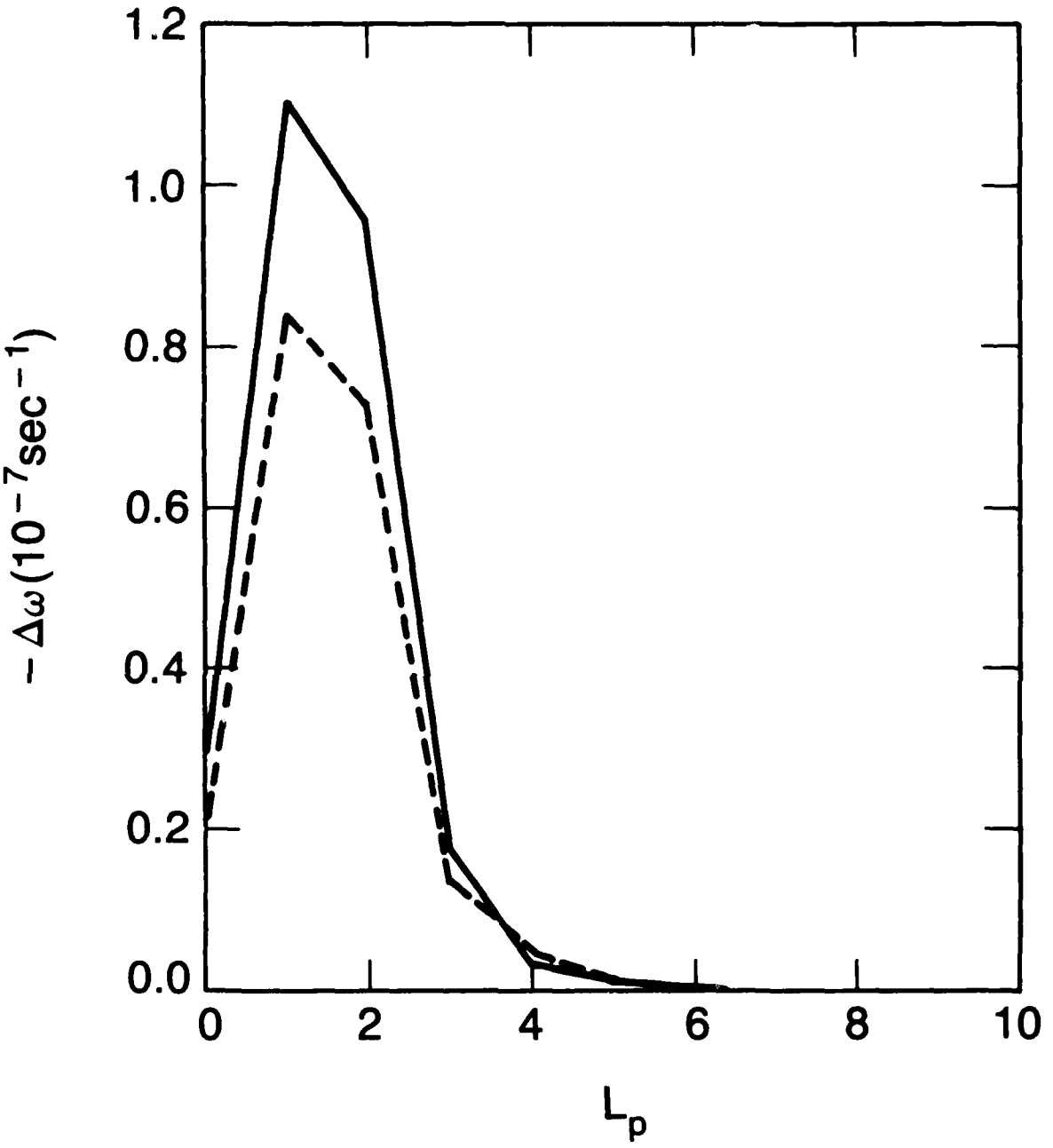


Fig. 14. Partial contributions to the Lyman-alpha shift of $He^+$ from total angular momenta $L_p$. Contributions correspond to line A (Fig. 6). Solid line: kT=2 eV; dashed line: kT=4 eV.

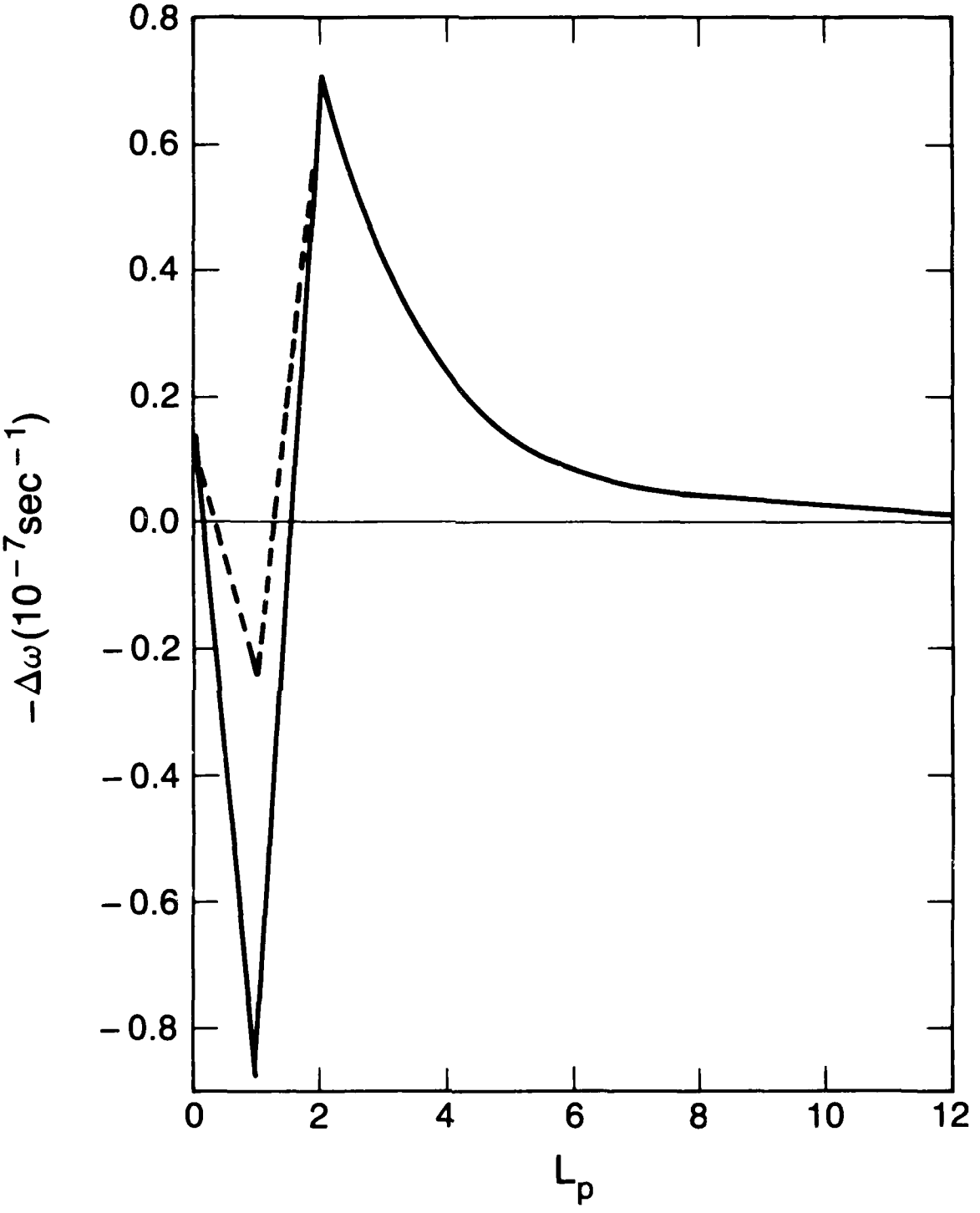


Fig. 15. Partial contributions to the Lyman-alpha shift of hydrogen from total angular momenta $L_p$. Contributions correspond to line A (Fig. 10). Solid line: kT=0.5 eV; dashed line: kT=2 eV

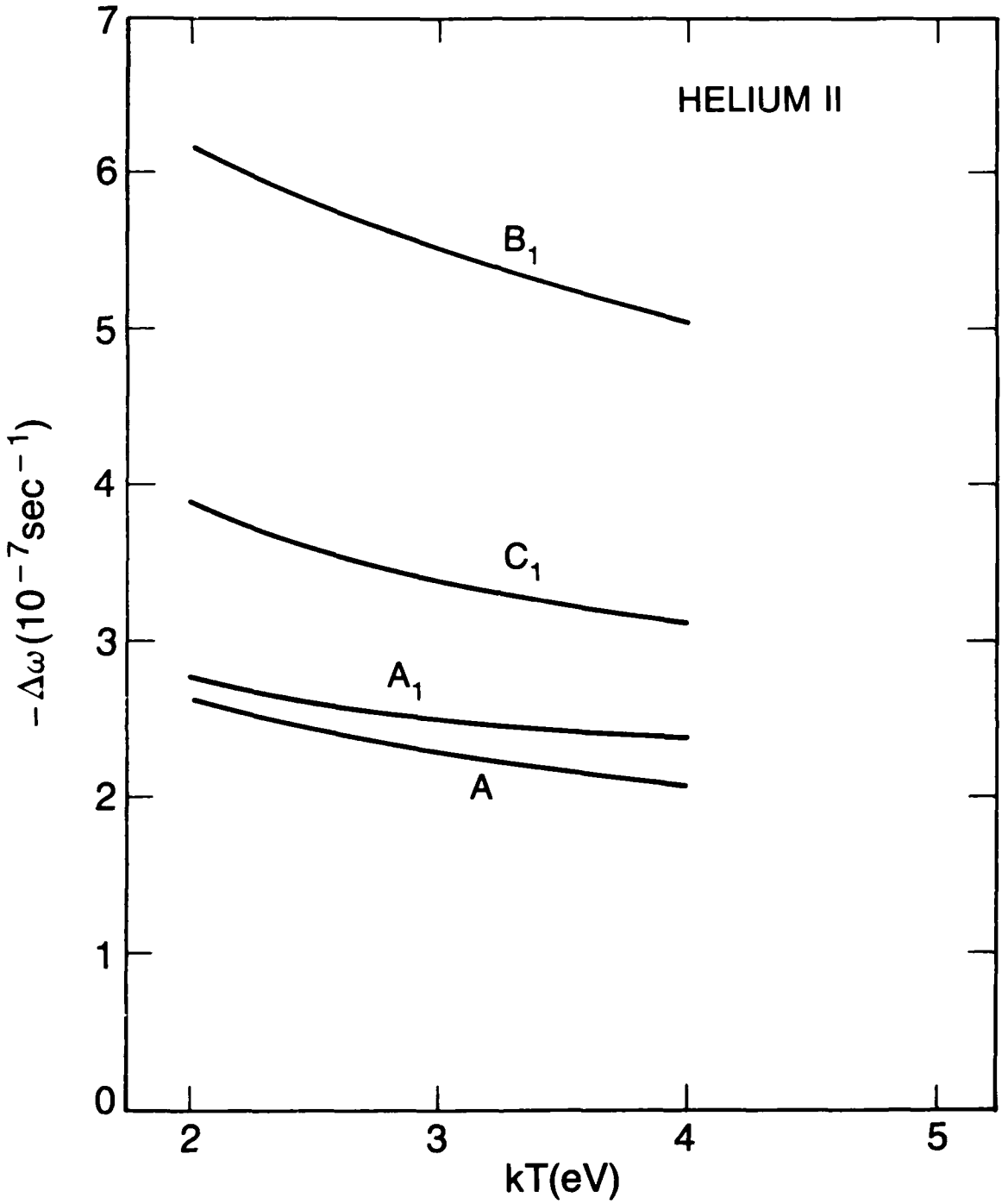


Fig. 16. Lyman-alpha shift of $He^+$.

A - DWX calculation (see Table 1);

$A_1$ - same as A with inclusion of second-order terms according to (27) except for contributions corresponding to the 2p-2s transition;

$B_1$ - same as A with inclusion of all second-order terms (contributions corresponding to 2p-2s transition included only up to $L^T=13$);

$C_1$ - $A_1$ plus contributions from 2p-2s transition taken from Griem[21].

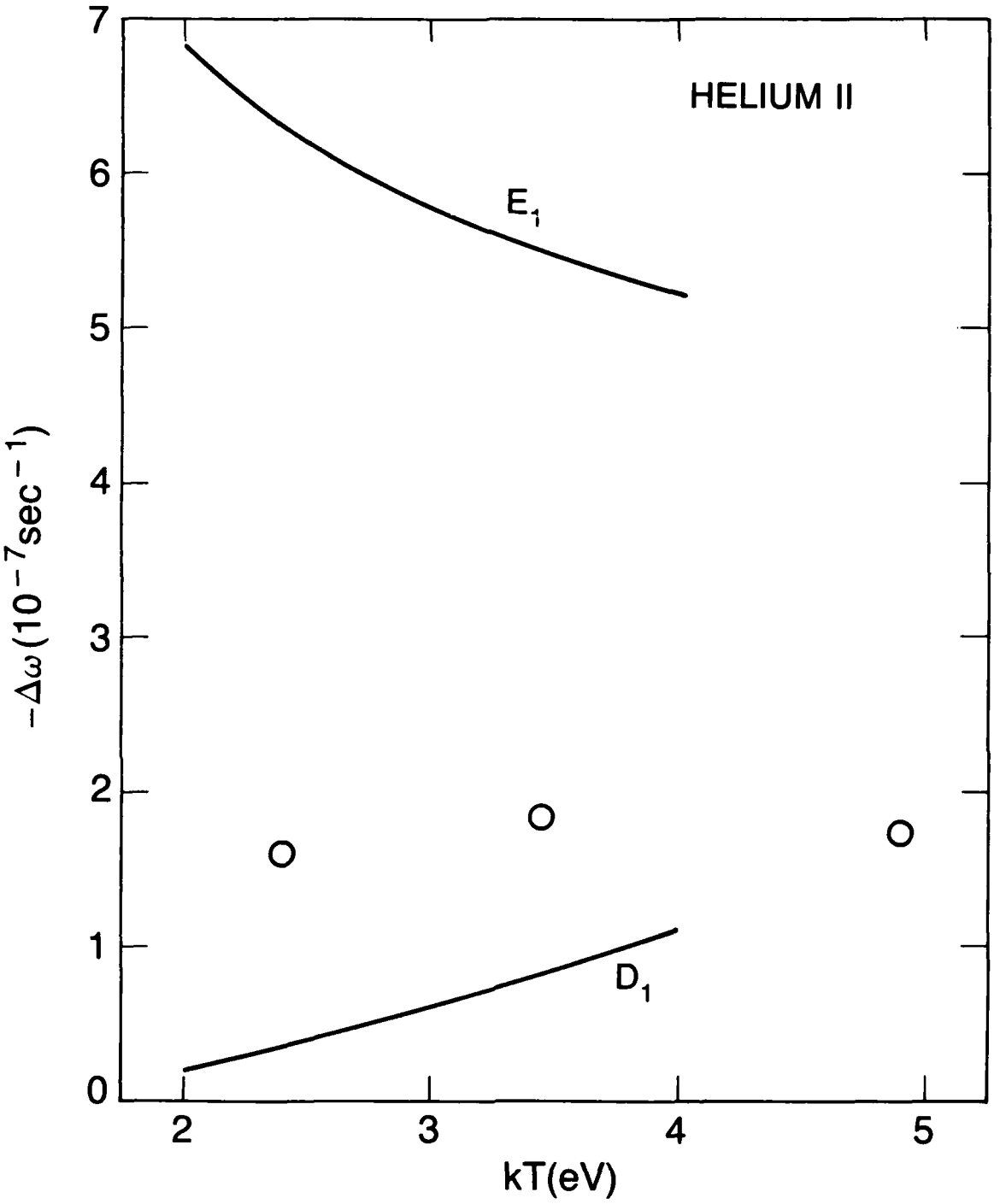


Fig. 17. Lyman-alpha shift of $He^+$.

$D_1$ - unitarized Coulomb-Bethe approximation with second-order terms according to (27). Only contributions corresponding to 2p-3s and 2p-3d transitions included;

$E_1$ - same as $D_1$, but elements of the $\rho$ matrix below the n=3 threshold set equal to the value of corresponding elements at the threshold;

circles: semi-classical approximation of Griem[3].

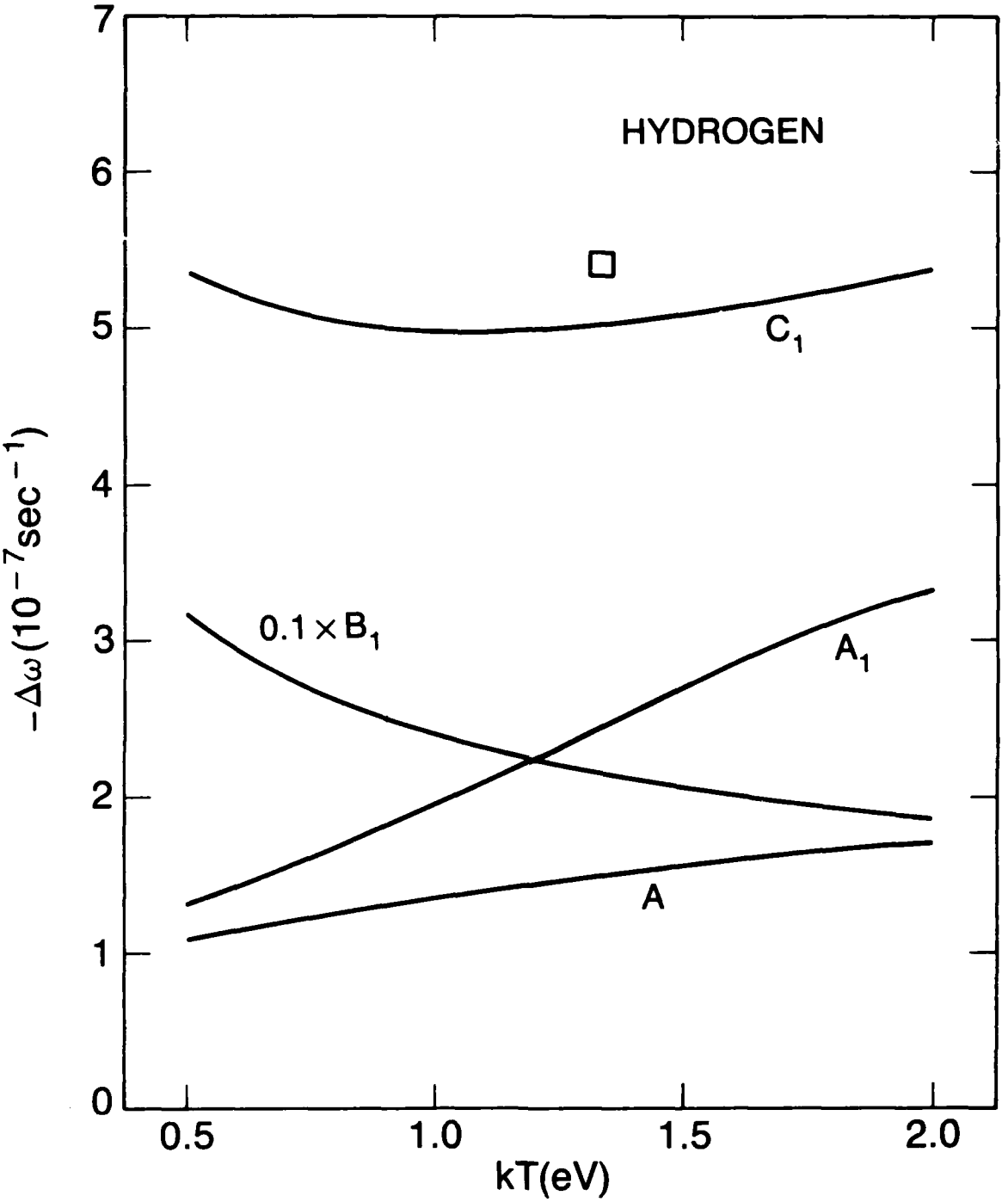


Fig. 18. Lyman-alpha shift of hydrogen.
A, $A_1$, $B_1$, $C_1$ - see caption to Fig. 16;
square - measured shift[23] corrected for ion contributions.

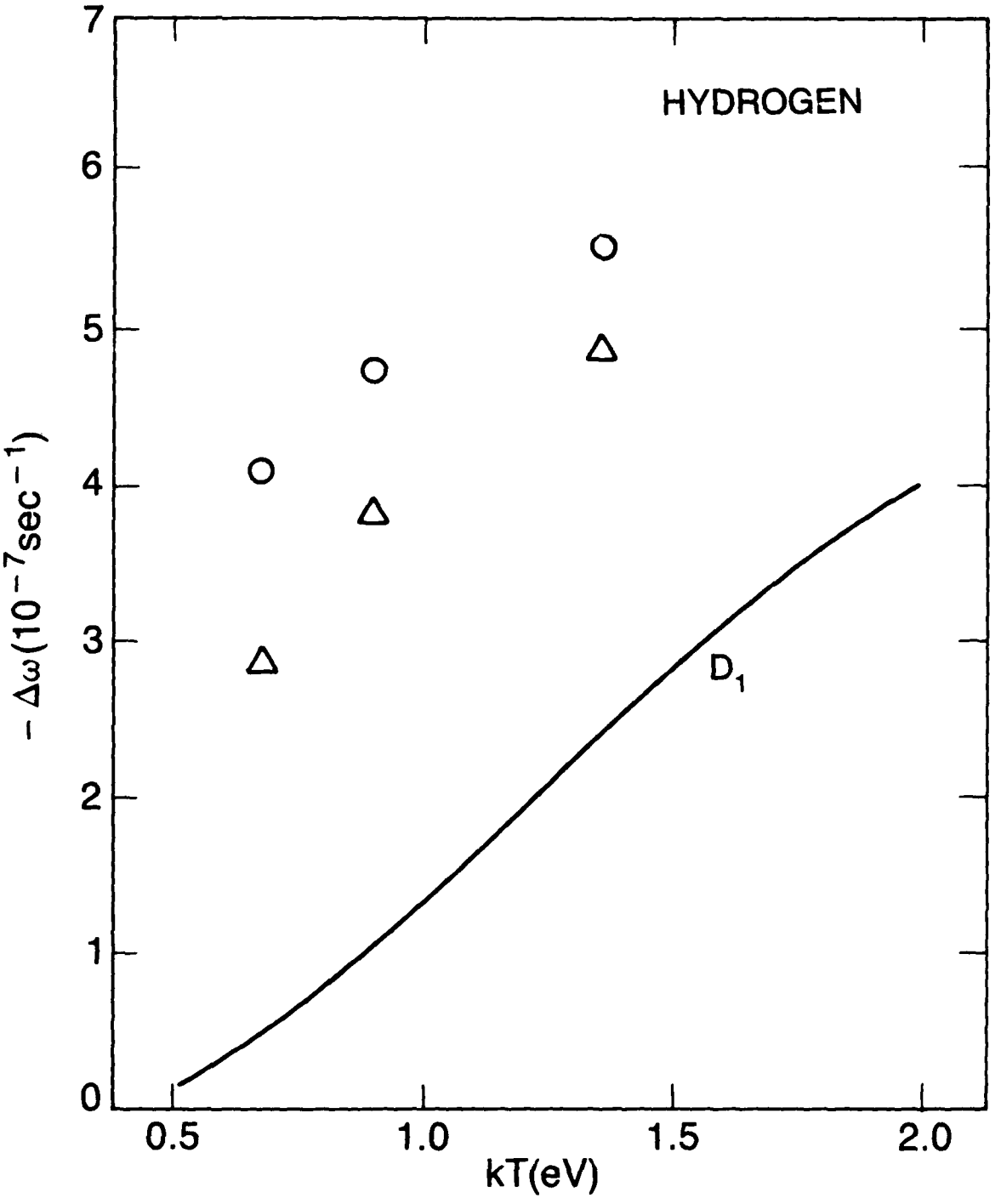


Fig. 19. Lyman-alpha shift of hydrogen.

$D_1$ - unitarized Bethe approximation with second-order terms according to (27). Only contributions corresponding to 2p-3s and 2p-3d transitions included;

circles: SC approximation of *Griem*[16] ($\Delta n=1$ contributions only);

triangles: same as circles without contributions from energies below n=3 threshold.

DISTRIBUTION LIST

Larry Altgilbers
3805 Jamestown
Huntsville, AL 35810

Argonne National Lab
9700 S. Cass Avenue
Argonne, IL 60439
Attn: Y. K. Kim
K. T. Lu, K105

Lloyd Armstrong
Department of Physics
Johns Hopkins University
Baltimore, MD 21318

P. Bakshi
Dept. of Physics and
Center for Energy Research
Boston College
Chestnut Hill, MA 02167

C. F. Barnett
Oak Ridge Natl. Lab
P.O. Box X
Bldg. 6003
Oak Ridge, TN 37830

Rogers Bengston
Dept. of Physics
U. of Texas
Austin, TX 78712

Klaus H. Berkner
Lawrence Berkeley Lab
Univ. of California
Berkeley, CA 94530

Nat Bhaskar
Columbia University
Columbia Radiation Lab
New York, NY 10027

Prof. L.C. Biedenharn
Duke University
Dept. of Physics
Durham, NC 27706

Howard C. Bryant
Phsyics and Astronomy
Univ. of New Mexico
Albuquerque, NM 87131

J. T. Chan
Physics Department
Univ. of Arkansas
Fayetteville, AK 72701

Edward S. Chang
Dept. of Physics
Univ. of Massachusetts
Amherst, MA 01003

Shih-I Chu
Dept. of Chemistry
Univ. of Kansas
Lawrence, KS 66045

David A. Clark
Univ. of New Mexico
P.O. Box 608
Albuquerque, NM 87544

E. D. Commins
Dept. of Physics
Univ. of California
Berkeley, CA 94720

William E. Cooke
Dept. of Physics
Univ. of S. California
University Park
Los Angeles, CA 90007

Stuart Crampton
Williams College
Williamstown, MA 01267

William A. Davis
Fusion Energy Division
Oak Ridge National Lab
Box Y, Bldg. 9201-2
Oak Ridge, TN 37830

Hans G. Dehmelt
Department of Washington
Univ. of Washington
Seattle, WA 98195

Alan Desilva
University of Maryland
Physics Dept.
College Park, MD 20742

Richard D. Deslattes
National Science Foundation
Washington, DC 20234

Norval Fortson
University of Washington
Seattle, WA 98105

Frank Franz
Dept. of Physics
Indiana University
Bloomington, IN 47405

Richard Freeman
Bell Laboratories
4D-321
Crawfords Corner Road
Homdel, NJ 07733

Robert S. Freund
Bell Laboratories
600 Mountain Avenue
Murray Hill, NJ 07974

G. Gerdin
214 Nucl. Eng. Lab.
1035 Goodwin
Urbana, IL 61801

K. I. Golden
Dept. of Electrical Engineering
University of Vermont
Burlington, VT 05401

Harvey Gould
Bldg. 70, Room 257
Lawrence Berkeley Lab
Berkeley, CA 94720

Hans Griem
University of Maryland
Lab. for Plasma & Fusion Studies
College Park, MD 20742

R. Gupta
University of Arkansas
Dept. of Physics
Fayetteville, AK 72701

Harvard University
60 Garden Street
Cambridge, MA 02138
W. H. Parkinson
Center for Astrophysics
Alex Dalgarno
Lyman Laboratory
Francis M. Pipkin

Roger A. Hegstrom
Dept. of Chemistry
Wake Forest University
Winston-Salem, NC 27109

Robert M. Hill
SRI International
333 Ravenswood Avenue
Menlo Park, CA 94025

Harry Jacobson
Dir. of Special Programs
University of Tenn.
Knoxville, TN 37916

Duane H. Jaecks
Physics Dept.
University of Nebraska
Lincoln, NE 68588

Thomas H. Jeys
Rice University
Space Phys. and Astronomy
6100 South Main
Houston, TX 77005

JILA/NBS
Campus Box 440
Univ. of Colorado
1510 Eisenhower Drive
Boulder, CO 80309
J. Cooper (1 each)
Sidney Geltman
Stephen J. Smith

Charles E. Johnson
Physics Dept.
N. Carolina State Univ.
Raleigh, NC 27607

W. R. Johnson
Physics Dept.
Univ. of Notre Dame
Notre Dame, IN 46556

B. R. Junker
ONR Code 323
800 North Quincy Street
Arlington, VA 22217

G. Kalman
Dept. of Physics and
Center for Energy Research
Boston College
Chestnut Hill, MA 02167

Kansas State University
Physics Dept.
Manhattan, KA 66506
Chander P. Bhalla
C. D. Lin

University of Virginia
Physics Dept.
McCormick Road
Charlottesville, VA 22901
Hugh R. Kelly
Tom Gallagher

KMS Fusion, Inc.
P.O. Box 1567
3621 S. State Road
Ann Arbor, MI 48106
George Charatis
Jon T. Larsen
Paul Rockett
D. Tanner

Joseph J. Kubis
P.O. Box 1082
Ann Arbor, MI 48106

Lawrence Livermore National Lab.
P.O. Box 808
Livermore, CA 94550
Attn: David Boercker, MS 387
Hugh E. DeWitt
Richard Fortner, L-401
Forrest J. Rogers
Balazs F. Rozsnyai, L-71
James H. Scofield
Bruce W. Shore

Los Alamos National Lab.
P.O. Box 1663
Los Alamos, NM 87545
Attn: Fred Begay (1 each)
John H. Brownell, MS 220
Lee A. Collins
C. W. Cranfill, MS 538
R. Godwin, MS 420
Alan Hauer, MS 554
Walter F. Huebner, MS 212
Joseph B. Mann
A. L. Merts
T. F. Stratton

Massachusetts Institute of
Technology
Cambridge, MA 02139
Shaoul Ezekiel
Rm. 26-255
Michael Feld
Rm. 6-009
Daniel Kleppner
Rm. 26-231

Harold J. Metcalf
Physics Dept
State University of NY
Stony Brook, NY 11794

Fred W. Meyer
Oak Ridge National Lab
P.O. Box X
Bldg. 6003
Oak Ridge, TN 37830

Masataka Mizushima
Physics Dept.
Univ. of Colorado
Boulder, CO 80309

National Bureau of Standards
Washington, DC 20234
Attn: Larry Roszman (1 each)
Joseph Reader
Raju U. Datla, Bldg. 221
Wofgang Wiese
Bldg. 221, Rm. A267

Univ. of Illinois
Dept. of Physics
Urbana, IL 61801
Attn: M. H. Nayfeth
Chicago Campus
C. Rhodes

Randolph S. Peterson
Box U-46
Dept. of Physics
Univ. of Conn.
Storrs, CT 06286

Robert Peterson
Nuclear Engineering Dept.
University of Wisconsin
1500 Johnson Drive
Madison, Wisconsin 53706

Physics International Inc.
2700 Merced Street
San Leandro, CA 94577
Richard L. Schneider
M. Krishnan

H. Pilloff
ONR Code 323
800 N. Quincy St.
Arlington, VA 22217

Michael S. Pindzola
Oak Ridge National Lab
Phys. Div., Bldg. 6003
Oak Ridge, TN 37830

Princeton University
Plasma Physics Laboratory
Forrestal Campus
Princeton, NJ 08540
Manfred L. Bitter
Kenneth W. Hill

A. K. Rajagopal
Dept. of Physics and Astronomy
Louisianna State Univ.
Baton Rouge, LA 70803

M. Eugene Rudd
University of Nebraska
Behlen Lab of Physics
Lincoln, NB 68588

D. H. Sampson
Dept. of Astronomy
525 Davey Laboratory
Pennsylvania State Univ.
University Park, PA 16802

Eugene J. McGuire
Org. 4211
Sandia Laboratories
P.O. Box 5800
Albuquerque, NM 87185

Wolfgang Sandner
SRI International
332 Ravenswood Avenue
Menlo Park, CA 94025

Ivan A. Sellin
Oak Ridge National Lab
P.O. Box X
Oak Ridge, TN 37830

Robin Shakeshaft
Dept. of Physics
Texas A & M Univ.
College Station, TX 77843

R. Shepherd
Dept. of Nuclear Eng.
114 N.A.M.E.
Ann Arbor, MI 48106

Haward A. Shugart
Dept. of Physics
Univ. of CA
Berkeley, CA 94720

Rolf Sinclair
Physics Division
Natl. Sci. Foundation
Washington, DC 20550

Ken Smith
Rice Univ.
Space Phys. and Astronomy
6100 South Main
Houston, TX 77005

Winthrop W. Smith
Dept. of Physics
Univ. of Conn.
Storrs, CT 06268

Larry Spruch
New York University
Physics Dept.
4 Washington Place
New York, NY 10003

Stanford University
Stanford, CA 94305
ATTN: Nils Carlson (1 each)
S. E. Harris
Edward L. Ginzton Lab
W. E. Meyerhof
Arthur L. Schawlow

Ronald F. Stebbings
Dept. of Space and Astron.
Rice Univ.
Houston, TX 77001

Rudolph M. Sternheimer
Dept. of Physics
Brookhaven National Lab.
Upton, NY 11973

Strategic Defense Initiative Org.
Pentagon
Washington, DC 20301-7100
Attn: Dwight Duston/IST
Len Caveny/IST

C. F. Hooper, Jr.
University of Florida
Dept. of Physics
Gainesville, FL 32611

University of Michigan
Physics Dept.
500 E. University
Ann Arbor, MI 48109
Attn: W. L. Williams
Jens C. Zorn
T. Kammish
Dept. of Nucl. Eng.

University of Rochester
Lab. for Laser Energetics
250 E. River Road
Rochester, NY 14623
Reuben Epstein
Stanley Skupsky

University of Pittsburgh
Pittsburgh, PA 15260
Attn: J. E. Bayfield
100 Allen Hall
Physics Dept.
Richard H. Pratt

L. Vahala
Dept. of Elec. Eng.
Old Dominion University
Norfolk, VA

Carol Venanzi
Ritgers University
P.O. Box 939
Piscataway, NJ 08854

Leposava Vuskovic
Jet Propulsion Lab
4800 Oak Grove Drive
Pasadena, CA 91103

Fred L. Walls
Natl. Bur. of Standards
325 Broadway
Boulder, CO 80303

Shinichi Watanabe
Dept. of Physics
University of Chicago
1100 East 58th St.
Chicago, IL 60637

William Westerveld
Dept. of Physics
N. Carolina State Univ.
Raleigh, NC 27650

William Wing
Phys. and Optical Sciences
University of Arizona
Tucson, AZ 85721

Peter Winkler
Physics Dept.
University of Nevada
Reno, Nevada 89557

David M. Woodall
Dept. of Nuclear Engineering
University of New Mexico
Albuquerque, NM 87131

Robert Yaris
Chemistry Department
Washington University
St. Louis, MO 63130

Pierre Agostini
C.E.A.
CEN SACLAY
B.P. 2 Gif-sur-Yvette
FRANCE

Ignacio Alvarez
Instituto de Fisica
U.N.A.M.
Apdo. Pstal 20-364
MEXICO

Dr. Alain Angelie
Commissarait a l'Energie Atomique
Villeneuve St. Georges
FRANCE

Alain Aspect
Universite Paris Sud
B.P. 43
91406 Orsay Cedex
FRANCE

P.E.G. Baird
Clarendon Laboratory
University of Oxford
Parks Road
Oxford, ENGLAND

Gunter G. Baum
Univ. Bielefeld
Fakultat fur Physik
48 Bielefeld
WEST GERMANY

Uwe Becker
Tech. Univ. Berlin
Rondellstr. 5, D-1000
Berlin 37
WEST GERMANY

Biblioteque
21, Av. des Bains
CH-1007 Lausanne
SWITZERLAND

Emile Biemont
Inst. D'Astrophysique
Universite de Liege
B-4200 Cointe-Ougree
BELGIUM

C. Bouchist
Ecole Normale Sup.
24 Rue Lhomond 24
75231 Paris Cedex 05
FRANCE

Fritz Buchinger
Mainz University
CERN
CERN Div. EP
Geneve, SWITZERLAND

D. D. Burgess
The Blackett Laboratory
Imperial College of Sci. and Tech.
London SW7 2BZ
ENGLAND

Carmen Dra. Cisneros
Instituto de Fisica
U.N.A.M.
Apdo. Postal 20-364
MEXICO

Charles W. Clark
SRC Daresbury Lab.
Daresbury, Warrington
ENGLAND WA4 4AD

N. Czsjkowski
University of Windsor
Windsor, Ontario
CANADA N9B 3P4

C. Deutsch
Laboratoire de Physique des Plasmas
Universite Paris XI
91405 Orsay
FRANCE

Andre Dietrich
Tech. Univ. Berlin
D 1 Berlin 37
Rondellstrasse 5
WEST GERMANY

Gordon Drake
Dept. of Physics
Univ. of Windsor
Windsor, Ontario
CANADA N9B 3P4

Francoise Fabre
C.E.A.
CEN SACLAY
B.P.2 Gif-sur-Yvette

FRANCE
Edmond Genenx
Universitat Bern
Sidlerstrasse
3012 Berne
SWITZERLAND

Elisabeth Giacobino
Universite Paris VI
4 Place Jussieu
75230 Paris Cedex 05
FRANCE

Samuel A. Goldman
University of Windsor
Windsor, Ontario
CANADA N9B 3P4

Dr. Francois Grimaldi
Centre d'Etudes de Limeil
Villeneuve, St. Georges
FRANCE

G. Friedrich Hanne
Physikal Institut
Correnssstrasse
4400 Muenster
WEST GERMANY

R. A. Holt
Dept. of Physics
Univ. of West. Ontario
London, Ontario
CANADA N6A 3K7

J. W. Humberston
Univ. College London
Gower Street
London WC1E 6BT
ENGLAND

F. E. Irons
Hughes Technology Pty. Ltd.
P.O. Box 1155
Canberra
A.C.T. 2601
AUSTRALIA

P. Jaegle
Laboratoire de Spectroscopie
Atomique et Ionique
University Paris-Sud
Orsay, FRANCE

Dr. Takao Kato
Institute of Plasma Physics
Nagoya University, JAPAN

H. Klein
Clarendon Laboratory
Parks Road
Oxford
ENGLAND

Hans Kleinpoppen
Inst. of Atomic Phys.
University of Stirling
Stirling, FK94LA
ENGLAND

Aaron D. Krumbein
Soreq Nuclear Research Center
Yavne, ISRAEL 70600

Hans-Joach I. Kunze
Inst. Experimentalphysik v
Ruhr Universitat
Postfach 2148
4630 Bochum
WEST GERMANY

Dr. Michele Lamoureux
Laboratoire de Spectroscopie
Atomique et Ionique
Universite Paris-Sud
Orsay, FRANCE

W. N. Lennard
Atom. Ener. of Canada Ltd.
C.R.N.L.
Chaulk River, Ontario
CANADA KOJ 1JO

Librarian
Max-Planck-Institut fur
Plasmaphysik
8046 Garching bei Munchen
WEST GERMANY

Library
Institut fur Plasmaforschung
Universitat Stuttgart
Pfaffenwaldring 31
700 Stuttgart 80
WEST GERMANY

H.O. Lutz
Univ. bielefeld
Fakultat fur Physik
D-4800 Bielefeld 1
WEST GERMANY

Dr. M. Stuart McRobert
Blackett Laboratory
Imperial College
ENGLAND

Reinhard Morgenstern
University Utrecht
Princetonplein 5
NL 3508 TA Utrecht
NETHERLANDS

Hajime Narumi
Dept. of Physics
Hiroshima University
Hiroshima 730
JAPAN

A. Ng
Dept. of Physics
U.B.C. Vancouver
B.C., CANADA V6T 1W5

Derek Paul
Physics Dept.
University of Toronto
Toronto M5S 1A7 CANADA

Dr. F. Perrot
Centre d'Etudes de Limeil
Villeneuve St. Georges
FRANCE

F. H. Read
Physics Dept.
Univ. of Manchester
Manchester M13 9P1
ENGLAND

Arne Rosen
Dept. of Physics
Chalmers Univ. of Tech
S-41296 Goteborg
SWEDEN

S. David Rosner
Dept. of Physics
Univ. of Western Ontario
London, Ontario
N6A 3K7 CANADA

David Salzmann
Soreq Nuclear Research Center
Yavne 70600
ISRAEL

Joshua D. Silver
Univ. of Oxford
Parks Road
Oxford OX1 3PU
ENGLAND

A.C.H. Smith
Dept of Phys. and Astro.
Univ. College London
London EC1E 6BT
ENGLAND

N. Stolterfoht
Hahn-Mfitner-Institut
D-1 Berlin 39
100 Glienickerstr.
WEST GERMANY

J.D. Talman
Dept. of Chemistry
Univ. of West Ontario
London, Ontario
N6A 3K7 CANADA

Hiroshi Tanaka
Sophia University
Faculty of Sci. and Tech.
Chiyoda-Ku, Koiocho 7
Tokyo, JAPAN 102

F. Trager
Physikalisches Institut
Der Univ. Heidelberg
D-690 Heidelberg 1
WEST GERMANY

Ervin Weinberger
University of Toronto
255 Huron St.
Toronto, Ontario
CANADA M5S 1A7

Tatsuhiko Yamaneka
Osaka University
Osaka, JAPAN

Dieter Zimmermann
Inst. fur Strahlungs-Un
Kerenphysik
Technische Univ. of Berlin
D-1002 Berlin
WEST GERMANY

Zev Zinzmon
The Weizmann Insitute of Science
Rohovot, ISRAEL

Naval Research Laboratory
Washington, D. C. 20375-5000
Code 4700 26 copies
*Code 4720 50 copies*
P. Burkhalter, Code 4681
Ed McClean, Code 4732
Dave Nagel, Code 4700

DIRECTOR OF RESEARCH
U.S. NAVAL ACADEMY
ANNAPOLIS, MD 21402 2 copies

CODE 1220 1 copy

CODE 2628 22 copies

Records 1 copy

Cindy Sims (Code 2634) 1 copy